



1 **Evaluation of biomass burning aerosols in the HadGEM3**
2 **climate model with observations from the SAMBBA field**
3 **campaign**

4

5 B. T. Johnson¹, J. M. Haywood^{1,2}, J. M. Langridge¹, E. Darbyshire³, W. T. Morgan³, K.
6 Szpek¹, J. Brooke¹, F. Marengo¹, H. Coe³, P. Artaxo⁴, K. M. Longo⁵, J. Mulcahy¹, G. Mann⁶,
7 M. Dalvi¹, and N. Bellouin⁷

8

9 ¹Met Office, Exeter, UK

10 ²CEMPS, University of Exeter, Exeter, UK

11 ³Centre for Atmospheric Science, University of Manchester, Manchester, UK

12 ⁴Physics Institute, University of São Paulo, São Paulo, Brazil

13 ⁵National Institute for Space Research (INPE), São José dos Campos, Brazil

14 ⁶National Centre for Atmospheric Science, School of Earth and Environment, University of
15 Leeds, Leeds, UK

16 ⁷Department of Meteorology, University of Reading, Reading, UK

17

18 Correspondence email: ben.johnson@metoffice.gov.uk

19



1 **Abstract**

2 We present observations of biomass burning aerosol from the South American Biomass
3 Burning Analysis (SAMBBA) and other measurement campaigns, and use these to evaluate
4 the representation of biomass burning aerosol properties and processes in a state-of-the-art
5 climate model. The evaluation includes detailed comparisons with aircraft and ground data,
6 along with remote sensing observations from MODIS and AERONET. We demonstrate
7 several improvements to aerosol properties following the implementation of the GLOMAP-
8 mode modal aerosol scheme in the HadGEM3 climate model. This predicts the particle size
9 distribution, composition and optical properties, giving increased accuracy in the
10 representation of aerosol properties and physical-chemical processes over the CLASSIC bulk
11 aerosol scheme previously used in HadGEM2. Although both models give similar regional
12 distributions of carbonaceous aerosol mass and Aerosol Optical Depth (AOD), GLOMAP-
13 mode is better able to capture the observed size distribution, single scattering albedo, and
14 Ångström exponent across different tropical biomass burning source regions. Both aerosol
15 schemes overestimate the uptake of water compared to recent observations, CLASSIC more
16 so than GLOMAP-mode, leading to a likely overestimation of aerosol scattering, AOD and
17 single scattering albedo at high relative humidity. Observed aerosol vertical distributions were
18 well captured when biomass burning aerosol emissions were injected uniformly from the
19 surface to 3km. Finally, good agreement between observed and modelled AOD was gained
20 only after scaling up GFED3 emissions by a factor of 1.6 for CLASSIC and 2.0 for
21 GLOMAP-mode. We attribute this difference in scaling factor mainly to different
22 assumptions for the growth of aerosol mass during ageing via oxidation and condensation of
23 organics.

24

25 **1 Introduction**

26 Biomass burning is a major source of tropospheric aerosol globally (van der Werf et al., 2010)
27 and dominates the aerosol burden in many tropical regions. Carbonaceous aerosols are
28 produced from open burning of vegetation, including both wild fires and managed fires for
29 clearing forest, pasture and arable land. These aerosols have a wide range of impacts
30 (Voulgarakis and Field, 2015) including short-term influences on local and regional weather
31 (e.g. Kolusu et al., 2015) and significant impacts on regional air quality and human health
32 (Johnston et al., 2012; Reddington et al. 2015). They also have a significant role in climate



1 change as they affect the global energy budget in a number of ways (e.g. IPCC, 2013; Bauer
2 and Menon 2012, Haywood and Boucher 2000).

3 The aerosols emitted from Biomass Burning (BB) are composed primarily of organic carbon
4 and black carbon and they both scatter and absorb solar radiation in the atmosphere. Such
5 “aerosol-radiation interactions” lead to large reductions of surface insolation and significant
6 radiative heating of the atmosphere (Ramanathan and Carmichael, 2008; Johnson et al.,
7 2008a; Malavelle et al., 2011; Milton et al., 2008). These effects can suppress the
8 hydrological cycle and influence regional atmospheric circulation affecting global
9 precipitation patterns (Wu et al., 2013; Ramanathan et al., 2001). The enhancement of
10 particulate numbers by BB can also increase the concentration of cloud condensation nuclei
11 modifying cloud microphysical properties (Spracklen et al., 2011). This can brighten clouds
12 (Twomey 1974) and modelling studies have also shown that smoke (aerosol) from BB can
13 delay the onset of precipitation and influence the evolution of convective clouds (Andreae et
14 al., 2004; Feingold et al. 2001). The localised heating associated with absorption of solar
15 radiation by the emitted particles can also suppress convection and change regional cloud
16 cover via the semi-direct aerosol effect (Koren et al., 2008; Tosca et al., 2014).

17 Quantifying the impact of BB aerosol emissions on the global radiation budget and climate is
18 therefore difficult with many competing effects and sources of uncertainty (Ten Hoeve et al.,
19 2012; Ward et al. 2012). Recent assessments suggest that on a global basis, changes in the top
20 of the atmosphere (TOA) radiation budget resulting from increased scattering due to aerosol
21 emitted from BB is approximately cancelled by increased absorption by the aerosol (Myhre et
22 al., 2013; Shindell et al., 2013; Bellouin et al., 2013). However, the extent to which scattering
23 and absorption compensate varies regionally as it depends on many factors including the
24 surface albedo, cloud cover, and the optical properties of the aerosol. In particular, the single
25 scattering albedo (e.g. Myhre et al., 2008), and the vertical distribution of the absorbing
26 aerosol relative to clouds (e.g. Samset et al., 2013) have a strong influence on this potential
27 balance. Absorption depends mainly on the black carbon content of the aerosol, but a
28 significant contribution in the UV, and to a lesser extent visible spectrum, can come from
29 organics, i.e. brown-carbon (Saleh et al., 2014).

30 Overall, BB aerosol emissions are estimated to lead to a global mean negative Effective
31 Radiative Forcing (ERF) as aerosol-cloud interactions in models are shown to exert a negative
32 forcing that outweighs any small positive forcing from aerosol-radiation interactions. This is



1 expected to have a cooling influence on global climate but the ERF and global temperature
2 responses are estimated to be relatively small, compared to those from sulphates or black
3 carbon from fossil fuel combustion (Jones et al., 2007; Shindell et al., 2013). Nevertheless,
4 increases in aerosol due to BB have potentially important impacts on regional climates, via
5 changes in atmospheric circulation and shifts in precipitation (Tosca et al., 2010, 2013; Ott et
6 al., 2010; Zhang et al., 2009; Jones et al., 2007).

7 Recent studies have also highlighted more complex Earth-system interactions associated with
8 BB emissions. By scattering solar radiation and increasing the ratio of diffuse to direct
9 radiation at the surface, aerosol can enhance photosynthesis over tropical forests, increasing
10 Net Primary Productivity (NPP) and carbon uptake (Rap et al., 2015; Mercado et al. 2009).
11 On the other hand, tropospheric ozone produced due to NO_x emissions from fires can damage
12 plants, reducing NPP (Pacifico et al. 2015). Mao et al. (2013) also showed that emission of
13 aerosol and trace gases from BB led to increases in global tropospheric ozone and methane
14 lifetime. In their study this led to a positive radiative forcing that offset the negative radiative
15 forcing from the sum of aerosol-radiation and aerosol-cloud interaction effects.

16 Quantifying these wide-ranging impacts of BB on climate, air quality and the earth-system
17 relies on the accurate representation of BB processes and aerosol properties in global models.
18 It is therefore important to evaluate their simulation in models with observations to reduce
19 inherent biases and identify priorities for future improvements to emissions, processes and
20 techniques used to represent aerosol properties. The properties of aerosols in BB-dominated
21 air masses have been investigated during a number of field experiments (e.g. Kaufmann et al.,
22 1998; Swap et al., 2002; Haywood et al., 2008), and reviewed by Reid et al. (2005a, 2005b)
23 and Martin et al. (2010). A new set of observations is now available from the South American
24 Biomass Burning Analysis (SAMBBA), a field campaign that took place in Brazil during 14
25 September – 4 October 2012. The measurement campaign was a joint UK-Brazil project led
26 by the Met Office and NERC, in collaboration with the National Institute of Space Studies in
27 Brazil (INPE) and University of Sao Paulo (USP) in Brazil. The campaign involved the UK
28 Facility for Airborne Atmospheric Measurements (FAAM) BAe-146 atmospheric research
29 aircraft coordinated with a range of ground-based observations (Allan et al., 2014; Brito et al.,
30 2014; Marenco et al., 2016). The airborne campaign comprised 20 flights investigating
31 aerosol properties, atmospheric chemistry, clouds, meteorology and the radiation budget over



1 Amazonia. The flights provided intensive measurement of aerosols across Amazonia
2 including aerosol dominated by BB emissions.

3

4 In this study we combined the observations from SAMBBA with those from previous
5 campaigns and from long-term remote sensing observations (MODIS, AERONET) to
6 evaluate the representation of Biomass Burning Aerosol (BBA) in a state-of-the-art global
7 climate model, the Hadley Centre Global Environment Model version 3 (HadGEM3). We
8 evaluate two aerosol schemes: (i) the mass-based CLASSIC aerosol scheme, (ii) the
9 microphysical scheme GLOMAP-mode. CLASSIC was previously used in HadGEM2-ES for
10 CMIP5 (Bellouin et al., 2011) and in this study is used within HadGEM3. GLOMAP-mode
11 has been implemented more recently in the Met Office Unified Model and is available in
12 HadGEM3 (e.g. Bellouin et al., 2013) (in some publications configurations of HadGEM3 that
13 include GLOMAP-mode have been referred to as HadGEM-UKCA). The study focuses on
14 aerosol properties important in simulating aerosol-radiation interactions, including the global
15 distribution of aerosol and their physical, chemical and optical properties. The study provides
16 an assessment of the influence of biomass burning on aerosol properties, as simulated by each
17 scheme, and assesses some of the assumptions commonly used to represent BB aerosol
18 emissions and aerosol processes in global models.

19 **2 Methods**

20 **2.1 HadGEM3 model configuration**

21 This work uses global simulations of the Met Office Unified Model (MetUM) within the
22 framework HadGEM3 (Hewitt et al., 2011). The scientific configuration of the physical
23 model was from the Global Atmosphere 7 (GA7) configuration and our simulations ran with a
24 resolution of N96 ($1.25^\circ \times 1.875^\circ$) and 85 vertical levels. Sea surface temperatures and sea ice
25 were prescribed using reanalysed daily-varying fields for the period 2002 – 2011 based on the
26 methodology of Reynolds et al. (2007) (as used in Atmosphere Model Intercomparison
27 Project). The atmospheric circulation was free-running including aerosol-radiative effects
28 from either CLASSIC or GLOMAP-mode. The atmospheric physics configuration includes
29 some updates to atmospheric processes over previous configurations presented in Williams et
30 al. (2015) and Walters et al. (2014). The main update affecting this study is the
31 implementation of the Global Model for Aerosol Processes (GLOMAP-mode) (Mann et al.,



1 2010) modal aerosol scheme. The implementation of GLOMAP-mode in the MetUM took
2 place as part of the UKCA (United Kingdom Chemistry and Aerosol) project along with
3 several alternative atmospheric chemistry schemes. In this study we use an offline-chemistry
4 configuration where concentrations of gas phase chemical species [ozone (O_3), hydrogen
5 peroxide (H_2O_2), and the hydroxyl (OH), nitrate (NO_3) and hydroperoxyl (HO_2) radicals]
6 required for the oxidation of aerosol precursor species are provided as monthly mean
7 climatologies. The climatology of oxidants was generated from a previous 20-year simulation
8 that included on-line gas-phase atmospheric chemistry using the UKCA combined
9 tropospheric and stratospheric chemistry scheme (O'Connor et al., 2014; Morgenstern et al.,
10 2009). For this study a parallel simulation was also run with the same model configuration
11 except that aerosols were simulated by the CLASSIC (Coupled Large-scale Aerosol Scheme
12 for Simulations in Climate Models) aerosol scheme. CLASSIC was the aerosol scheme used
13 in HadGEM2, including Hadley Centre contributions to the fifth Coupled Model
14 Intercomparison Project (CMIP5) (Bellouin et al., 2011). As in the GLOMAP-mode
15 simulation a climatology of oxidants was used, generated from previous simulations with the
16 UKCA atmospheric chemistry schemes. For both aerosol schemes fire emissions of BBA
17 were taken from the Global Fire Emission dataset (GFED) version 3.1 (van der Werf et al.,
18 2010). Details of how these were implemented are given in section 2.3. Anthropogenic
19 emissions of SO_2 and carbonaceous aerosol (from fossil fuel and bio-fuel) for both aerosol
20 schemes were based on the 10-year average emissions from 2002-2011. These data were
21 provided by MACC/CityZEN (via ECCAD-Ether at <http://eccad.sedoo.fr>) that interpolates
22 across this time frame using historical emissions for 2000 from ACCMIP (Lamarque et al.,
23 2010) and emissions for 2005 and 2010 from the RCP8.5 scenario (Granier et al. 2011; Diehl
24 et al., 2012). Volcanic degassing emissions of SO_2 were taken from Andres and Kasgnoc
25 (1998). Emissions of di-methyl sulphide (DMS) were calculated from the Kettle et al. (1999)
26 ocean DMS climatology with the Liss and Merlivat (1986) surface-exchange
27 parameterization. Stratospheric aerosol was represented via the climatology from Cusack et
28 al. (1998). Nitrate aerosols were not included in this study.



1 **2.2 Representation of aerosols**

2 **2.2.1 CLASSIC**

3 CLASSIC is a mass-based or “bulk” aerosol scheme that represents a range of aerosol species
4 (sulphate, fossil-fuel soot, fossil-fuel organic carbon, BBA, sea salt, and mineral dust) as
5 separate externally-mixed species with specified physical and optical properties. A full
6 description of the scheme is available in the appendix of Bellouin et al. (2011). CLASSIC
7 includes a representation of the sulphur cycle for the gas-phase and aqueous-phase production
8 of sulphate aerosol. Carbonaceous aerosols are represented as three separate species
9 depending on their emission source (soot, fossil-fuel organic carbon, BBA). Each has
10 different assumptions regarding their physical, chemical and optical properties. The
11 representation of the BBA species is based on the aircraft observations of Haywood et al.
12 (2003) and Abel et al. (2003) obtained over Southern Africa during SAFARI-2000 and is
13 described in more detail below. Mineral dust is simulated by the 6-bin scheme of Woodward
14 (2001), with modifications in Woodward (2011). CLASSIC uses a diagnostic scheme for
15 wind-driven sea salt, i.e. assumes no transport of sea salt aerosol over land. Secondary
16 Organic Aerosol (SOA) is not modelled explicitly by CLASSIC but the contribution to AOD
17 and radiative effects is included using an offline climatology. The SOA climatology is
18 provided by the UK Met Office Chemistry Transport Model (STOCHEM) (Derwent et al.
19 2003) based on the emission of isoprene from biogenic sources.

20 The BBA species includes a fresh mode to represent the primary particles, and an aged mode
21 to represent the aerosols after chemical ageing and growth. A third tracer is used to track the
22 mass of in-cloud BBA particles that are either lost via wet deposition or return to the aged
23 BBA mode as rain water is lost via evaporation. The size distribution for each mode is
24 represented by a single log-normal with a standard deviation of 1.3 and mean diameter of
25 $0.2\mu\text{m}$ for the fresh mode and $0.24\mu\text{m}$ for the aged mode. These are assumed to be an internal
26 mixture of Black Carbon (BC) and Organic Carbon (OC) with an organic carbon mass
27 fraction of 91.5 % for the fresh mode and 94.6 % for the aged mode. The ageing process
28 occurs on a 6-hour e-folding timescale and during the transfer from the fresh to aged mode the
29 aerosol mass is increased by a factor of 1.62. This representation of aerosol ageing is based on
30 the evolution of aerosol properties in a large smoke plume observed during SAFARI-2000
31 (Abel et al., 2003). Optical properties are calculated from Mie theory with the Refractive
32 Index (RI) computed as the volume-weighted average of the BC and OC components



1 assuming an aerosol mass density of 1.35g/cm^3 for the OC and 1.7g/cm^3 for the BC. The RI
2 of the BC component is based on WCP (1983) ($1.75 - 0.44i$ at 550nm) and the RI of the OC
3 component is assumed to be $1.53 - 0.0i$ across the solar spectrum. This gives an RI of $1.54 -$
4 $0.025i$ for the fresh mode and $1.54 - 0.018i$ for the aged mode, in the mid-visible (550nm).
5 Both species are hygroscopic with empirical growth curves from Magi and Hobbs (2003)
6 (Section 3.5).

7 **2.2.2 GLOMAP-mode**

8 The GLOMAP-mode (Global Model for Aerosol Processes) scheme (Mann et al., 2010) has
9 an entirely different modelling philosophy to CLASSIC, being an aerosol microphysics
10 scheme including a size-resolved representation of the key processes which alter the particle
11 physical and chemical properties during its lifecycle (e.g. Mann et al., 2014). The
12 configuration of GLOMAP-mode in this study (GA7) includes four soluble modes
13 (nucleation, Aitken, accumulation, coarse) and one insoluble Aitken mode, and includes the
14 components of sulphates, particulate organic matter, black carbon and sea salt. Aerosol
15 particles within any given mode are assumed to be an internal mixture of the chemical
16 constituents in that mode. Particles within a mode can grow by condensation and coagulation.
17 Aerosol mass and number can also be transferred from smaller to larger modes, either via
18 coagulation between the modes, or as the diameter of particles within a mode exceeds the
19 specified limit for that mode (Mann et al., 2010). Insoluble Aitken particles also age as
20 sulphuric acid and oxidised organic vapours condense onto them and the aerosol are
21 transferred to the accumulation soluble mode when the coating exceeds 10 mono-layers.
22 Although GLOMAP-mode generally treats mineral dust within the modal framework, in the
23 same way as other aerosol components, a modal representation for mineral dust was not
24 included in the GA7 configuration of the atmospheric model. Therefore, dust was modelled
25 separately using the CLASSIC dust scheme as in Bellouin et al. (2013). The simulation with
26 GLOMAP-mode included primary aerosol emissions from biomass burning, bio-fuel and
27 fossil fuel combustion sources, interactive sea spray emissions, and sub-grid sulphate particle
28 formation (so-called “primary sulphate”), assumed to be 2.5 % of emitted SO_2 . The scheme
29 explicitly represents the secondary aerosol particle source from binary nucleation of sulphuric
30 acid vapour and water vapour following the nucleation rate of Kulmala et al. (1998).
31 Secondary organic aerosol (SOA) mass forms following the oxidation of emitted biogenic
32 Volatile Organic Compounds (bVOCs), and the SOA is added to existing particles. In these



1 simulations, the only SOA-producing bVOC is a lumped monoterpene species taking
2 emissions from Guenther et al., (1995). The monoterpene reacts with OH, NO₃ and O₃
3 assuming a 26 % molar yield to the particle phase.

4 Aerosol emissions from biomass burning are assumed to have an initial (emitted) size
5 distribution given by a log-normal with a mean diameter of 0.15µm and standard deviation of
6 1.59, as used by Stier et al. (2005) and consistent with the range of log-normal parameters
7 fitted to BB aerosol size distributions in Fig. C2 of Dentener et al. (2006). The ratio of BC to
8 OC varies interactively in GLOMAP-mode depending on mixing of these components from
9 the range of sources mentioned above. There is currently no representation for the
10 condensation of VOCs from BB onto the aerosol phase and so unlike in CLASSIC the growth
11 of aerosol mass from secondary aerosol formation during ageing occurs only via condensation
12 of sulphate and oxidised bVOC. The BC component in GLOMAP-mode is assumed to be
13 hydrophobic whereas the organic aerosol component is assumed to be hydrophobic only in
14 the insoluble mode(s), and hygroscopic in the soluble modes. Further details on the
15 hygroscopic growth are given in section 3.5. As in CLASSIC, aerosol optical properties are
16 calculated from Mie theory with RI computed by volume-weighted averages depending on the
17 mixture of components within any given mode. The RI of the BC component, as in
18 CLASSIC, is based on WCP (1983) and the OC component is assumed to be non-absorbing
19 with an RI of 1.5 – 0.0i across the solar spectrum. Aerosol mass density for BC and OC are
20 assumed to be 1.5g/cm³.

21 **2.3 Biomass burning aerosol emissions and scaling factors**

22 **2.3.1 Global emission scaling factor**

23 Fire emissions of BBA were taken from the Global Fire Emission Dataset (GFED) version 3.1
24 (van der Werf et al., 2010). Preliminary simulations with GFED3.1 emissions led to large
25 underestimates in modelled aerosol mass and AOD over tropical BB regions. Therefore, we
26 apply global scaling factors of 1.6 for CLASSIC and 2.0 for GLOMAP-mode (Table 1) to
27 increase the total BB aerosol emissions to give good agreement between modelled and
28 observed mid-visible AOD (see section 3.1). Note, scaling BB aerosol emissions to observed
29 AODs is explicit in top-down emission estimation methods such as the Quick Fire Emission
30 Dataset QFED (Darmenov and da Silva 2013) and the Fire Energetics and Emissions
31 Research (FEER) (Ichoku and Ellison 2014) and these lead to global total particulate matter



1 emissions approximately 2-3 times greater than GFED3.1 (Ichoku and Ellison 2014). Other
2 modelling studies have also found it necessary to apply global scaling factors to increase
3 aerosol emissions from BB sources to gain realistic AOD and/or particulate mass
4 concentrations (Kaiser et al., 2012; Marlier et al., 2013; Petrenko et al., 2012; Tosca et al.,
5 2013; Archer-Nicholls et al., 2016; Kolusu et al., 2015; Reddington et al., 2016). However,
6 we acknowledge that the discrepancy between modelled and observed AOD (prior to
7 emission scaling) could be due to other biases or missing processes in the models.

8 In the CLASSIC simulation the global scaling factor of 1.6 (Table 1) was applied to the total
9 mass emitted into the BBA tracer. For GLOMAP-mode a factor of 2.0 was applied to the BB
10 emissions of aerosol mass (both the OC and BC component) and number. The scaling used
11 here differs between the two aerosol schemes, and aims of doing so is to quantify the
12 magnitude of the discrepancy between modelled and observed AOD (prior to scaling), and
13 highlight the fact that the discrepancy depends on assumptions and processes internal to the
14 aerosol schemes themselves.

15 **2.3.2 Scaling of organic carbon to primary organic matter**

16 In this study emissions of the organic aerosol component are derived from the OC flux
17 provided by GFED3.1. As OC represents the mass of the carbon only, the contribution of
18 other elements (principally oxygen) to the total organic aerosol mass (i.e. Primary Organic
19 Matter POM) must be considered separately. In CLASSIC no scaling is applied to convert the
20 mass of OC to POM. In GLOMAP-mode OC is converted to POM assuming a POM:OC mass
21 ratio of 1.4 (Table 1). This conversion factor of 1.4 has been broadly used in atmospheric
22 models and was originally based on analysis of filter measurements of fresh urban emissions
23 from the 1970's onwards (see Turpin and Lim, 2001 and references therein). More recent
24 analyses of aerosol mass spectra (e.g. Aitken et al., 2008; Ng et al., 2010; Tiitta et al., 2014;
25 Brito et al., 2014) and preliminary analysis of airborne data from SAMBBA indicate
26 POM:OC ratios in the range 1.5 – 1.8 for fresh particles / near-source emissions from biomass
27 burning. Therefore, an upward adjustment from the 1.4 conversion factor widely assumed
28 may be warranted to more accurately simulate the aerosol mass emissions from BB. However,
29 the observations indicate considerable variability with aerosol age and source region with
30 POM:OC ratios increasing to 2.0-2.3 for aged and more highly oxidised aerosol. This
31 introduces considerable uncertainty in gauging a representative POM:OC for global models
32 where near-source ageing may not be represented.



1 **2.3.3 Growth of organic aerosol component during ageing**

2 In CLASSIC the condensation of VOCs onto BBA is represented in a simplified manner
3 increasing the aerosol mass by a factor of 1.62 (Table 1) when the fresh BB mode is
4 converted to the aged mode. This scaling factor is based on measurements from a large plume
5 during SAFARI-2000 (Abel et al. 2003). However, the evidence for growth of aerosol mass in
6 BB plumes is mixed. For example, Vakkari et al. (2014) concluded that oxidation and
7 subsequent secondary aerosol formation were important in the evolution of smoke plumes 2-4
8 hours after emission. In contrast, other studies based on aircraft measurements of aerosol
9 composition and emission ratios have shown no net mass gain, or even net loss of aerosol
10 mass between fresh and aged plumes, despite oxidation (chemical ageing). These studies
11 include measurements from West Africa (Capes et al. 2008), from SAMBBA (Morgan et al.
12 2012), and from a synthesis of the West African measurements with three other campaigns
13 (Jolleys et al., 2012). These suggest that evaporation of organic material after initial emission
14 outweighs or at least compensates for mass added due to secondary formation of organic
15 aerosol. The assumed growth in CLASSIC is therefore not fully supported by recent
16 observational analyses and is an aspect of the scheme that must be considered as we evaluate
17 the model.

18 The configuration of GLOMAP-mode here does not include secondary aerosol formation
19 from VOCs emitted by biomass burning, or the associated variation of POM:OC during
20 chemical ageing. This is acknowledged as a potentially large source of bias that may to some
21 extent necessitate the global emission scaling.

22 **2.3.4 Vertical injection height assumptions**

23 Smoke plumes can rise several kilometres before detraining into the atmosphere, although this
24 depends critically on fire size / heat flux and atmospheric stability (Freitas et al., 2007).
25 Regional assessments show that the majority of smoke plumes detrain in the boundary layer
26 with maximum plume heights typically below 2km, whereas vigorous plumes from some
27 large fires can extend into the free troposphere up to altitudes 6 km or more in exceptional
28 cases (Freitas et al., 2007; Kahn et al., 2008; Val Martin et al., 2010; Val Martin et al., 2012;
29 Sofiev et al., 2012; Tosca et al., 2011). During SAMBBA the concentration of aerosol was
30 generally highest in the lowest (2 – 3 km corresponding to the maximum height of the
31 atmospheric boundary layer) and declined rapidly with height above this (Marenco et al.,
32 2015; Darbyshire et al., in preparation, 2016a). Tenuous aerosol layers were frequently



1 observed in the mid-troposphere up to altitudes of 5 or 6 km but given the prevalence moist
2 convection during SAMBBA (mainly in the Western region) it was difficult to determine
3 whether these elevated layers related to plume injection heights or were the result of vertical
4 transport and detrainment from cumulus (in some cases pyrocumulus were also observed).

5 HadGEM3 does not include an explicit smoke plume-rise model but prescribes the vertical
6 profile of emissions depending on vegetation type provided by GFED. Following
7 recommendations from the 1st phase of AeroCom (see section 7 and Fig. 9 of Dentener et al.,
8 2006) fire emissions from peat fires, savannah and woodland are assumed to have small
9 plume rise and are emitted at the lowest model level, allowing sub-grid scale turbulence to
10 mix these through the boundary layer. Emissions from forest and tropical deforestation fires
11 are assumed to have more significant plume rise and are injected uniformly from the surface
12 to an assumed maximum injection height of 3km. These injection height assumptions were
13 used identically for both the CLASSIC and the GLOMAP-mode simulations to maintain
14 consistency.

15 **2.4 Experimental design of simulations**

16 Three simulations were completed, each with a 3 month spin up followed by a 10 year run
17 with emissions, SSTs and sea ice based on the years 2002-2011. These included simulations
18 with: (i) CLASSIC aerosols, (ii) GLOMAP-mode aerosols, (iii) GLOMAP-mode but with no
19 BB emissions. Simulation (iii) enables the contribution of BB emissions to AOD and aerosol
20 mass to be inferred from GLOMAP-mode. Apart from these changes in the simulation of
21 aerosols the scientific configuration of the atmospheric model was identical in all simulations.
22 In these simulations the atmospheric circulation was free-running (not nudged to
23 meteorological analyses) and so a ten year period is required to average over interannual
24 variability of meteorology. The selected time period 2002 – 2011 spans the last 10 years
25 where GFED3.1 data was available. One advantage of selecting this time period rather than
26 earlier years is that the GFED3.1 emissions benefit from inclusion of the burned area product
27 from Aqua MODIS from 2002 onwards. Unfortunately, the GFED3.1 data were not available
28 for 2012 (the period of the SAMBBA campaign). For this reason the evaluations against
29 aircraft campaign data in this study focus on the intrinsic properties of BBA (physical,
30 chemical and optical properties) that are expected to depend more on the vegetation and
31 burning practices in the observed regions than on year-to-year variability of burned area.



1 **2.5 In situ observations from SAMBBA and other biomass burning campaigns**

2 Aircraft measurements of aerosol properties have been taken from the SAMBBA campaign
3 that took place in Brazil during Sept-Oct 2012. As the aerosol properties differed regionally
4 (Darbyshire et al., in preparation, 2016b) we present average properties separately for the
5 Western region (flights based from Rondonia: 7-12.5°S, 58-65°W) and Eastern region (flights
6 over Tocantins: 10-12°S, 46.5-49°W) (Fig. 1). An overview of the flights and full details of
7 instrumentation are provided in Darbyshire and Johnson (2012) and data processing methods
8 will be described in Darbyshire et al. (in preparation, 2016b). Aircraft measurements have
9 also been taken from the Dust and Biomass Burning Experiment (DABEX) over West Africa
10 (7-15°N, 0-7°E) during Jan-Feb 2006 (Haywood et al., 2008; Johnson et al.; 2008) and from
11 the Met Research Flight C130 aircraft during the Southern African Regional Science Initiative
12 (SAFARI-2000) in Sept 2000 (Haywood et al. 2003) (15-25°S, 8-18°E). The boxes in Fig. 1
13 indicate the regions where the flights took place and where model data was averaged.

14 Common to each of the aircraft datasets is the use of a wing-mounted Passive Cavity Aerosol
15 Spectrometer Probe (PCASP) to measure aerosol particle size distributions, a TSI three
16 wavelength nephelometer (440, 550, 700nm) to measure aerosol scattering, and a single
17 wavelength Particle Soot Absorption Photometer (523nm) to measure aerosol absorption and
18 the SSA (when combined with the nephelometer). During SAMBBA the PCASP suffered
19 some instrument / electronic processing errors after the first four flights (B731-734).
20 Therefore, stringent quality checks on the data were employed to filter out affected data. After
21 this, approximately 16 hours of PCASP data were available from 8 flights, with 75 % of this
22 from the first four flights (B731-734) that focussed mainly on sampling aerosol dominated by
23 biomass burning emissions. During SAMBBA, PCASP measurements of aerosol size
24 distribution were supplemented by a GRIMM Optical Particle Counter (OPC), and a TSI
25 Scanning Mobility Particle Sizer (SMPS). The aerosol composition was also measured during
26 SAMBBA and DABEX. In both cases the sulphate mass and the Organic Aerosol (OA) (i.e.
27 total carbonaceous aerosol mass from POM and Secondary Organic Aerosol) were measured
28 by an Aerodyne Aerosol Mass Spectrometer (Capes et al., 2008). During SAMBBA the BC
29 mass was estimated from a Single Particle Soot Photometer and during DABEX the BC mass
30 was estimated from the PSAP assuming a mass absorption coefficient of $12\text{m}^2/\text{g}$. For each
31 flight campaign the aircraft observations have been averaged over all available measurements
32 taken in biomass burning conditions to provide campaign mean BB aerosol properties.



1 Ground-based observations of aerosol composition have also been used based on data
2 presented in Tiitta et al. (2014) from the Welgegund station in South Africa (Fig. 1). They
3 used an Aerosol Chemical Speciation Monitor to measure OA and sulphate and a Multi-Angle
4 Absorption Photometer to measure BC assuming a mass absorption coefficient of $6.6\text{m}^2/\text{g}$.
5 We take an average composition from their measurements in September 2010.

6 2.6 Remote sensing observations

7 MODIS AOD retrievals have been obtained from the Aqua satellite. In this study we use
8 monthly mean level 3 MYD08_M3 data products and to aid the evaluation we include the
9 AOD products from both collection 5.1 and collection 6. In the case of collection 5.1 the dark
10 target (Levy et al., 2007, 2010) and ocean algorithms (Remer et al., 2005) have been used
11 where coverage is available, and the Deep Blue algorithm (Hsu et al., 2004, 2006) has been
12 used for pixels over bright land surfaces where dark-target retrievals were not available. For
13 collection 6 the merged product (Sayer et al., 2014) has been used that combines retrievals
14 from all three algorithms and includes various refinements to each (Sayer et al., 2013; Levy et
15 al., 2013). The monthly mean data has been averaged over the period 2003-2012 to create
16 long-term monthly means.

17 AERONET data have also been used for direct sun retrievals of AOD and for inversion
18 products of aerosol size distribution and optical properties. Six sites with strong biomass
19 burning influence were selected for use in this study: Alta Floresta (Brazil), Mongu (Zambia),
20 Ilorin (Nigeria), Chiang Mai (Thailand), Jaribu (N. Australia), and Bonanza Creek (Alaska)
21 (Fig. 1). We used monthly mean products from the version 2 algorithm (Dubovik and King,
22 2000; Dubovik et al., 2006) and used level 2 products in all cases except Chiang Mai where
23 level 1.5 data was used as level 2 data coverage was limited. Level 1.5 data is not fully cloud-
24 screen and calibrated so may not be as reliable. Long-term monthly mean averages were
25 calculated for 2002-2011.

26 2.7 Averaging methods

27 The aircraft in-situ observations presented in this study have been averaged over all available
28 measurements in biomass burning dominated conditions in each campaign or campaign sub-
29 region, to provide representative “campaign-mean” values. The data averaging methods for
30 SAMBBA will be described in more detail in Darbyshire et al. (in preparation, 2016b). The



1 DABEX campaign-means are taken from the observations of aged aerosol layers in (Johnson
2 et al., 2008). SAFARI-2000 campaign-means are based on a compilation of aged aerosol
3 measurements, as detailed in Haywood et al. (2003). Inevitably, aircraft flight patterns do not
4 provide unbiased spatial and temporal sampling of the atmosphere and tend to favour
5 sampling aerosol layers with medium-high aerosol loadings. However, by averaging over
6 large volumes of data focussed on regional sampling these aircraft datasets can provide useful
7 constraints on the physical, chemical and optical properties of the aged aerosol. Wherever
8 comparisons are made with model data, they are based on the 10-year (long-term) monthly
9 mean output from the models (September for SAMBBA and SAFARI-2000, January for
10 DABEX). For comparison with aircraft measurements, the model data has been averaged over
11 the latitude and longitude ranges of the relevant flight regions (boxes in Fig. 1) and over 0 – 5
12 km; the typical altitude range of the observed aerosol layers. For the comparison with
13 Welgegend surface measurements model data is taken from the lowest model level of the grid
14 box co-located with the site and for September, corresponding to the peak of the BB season in
15 Southern Africa. For comparisons with AERONET the 10-year (long-term) monthly mean
16 model output is selected for the gridbox co-located with the AERONET site and averaged
17 vertically to provide column-mean aerosol properties.

18

19 **3 Evaluation of CLASSIC and GLOMAP-mode with observations**

20 **3.1 Aerosol optical depth**

21 **3.1.1 Global AOD evaluation with MODIS**

22 Fig. 2 assesses the contribution of biomass burning to annual mean Aerosol Optical Depth
23 (AOD) at the global scale. For CLASSIC the contribution of BB emissions to the total AOD
24 (hereafter BBAOD) is straightforward as carbonaceous aerosol originating from biomass
25 burning emissions are represented as separate (externally mixed) species in the model. For
26 GLOMAP-mode aerosols from different sources are internally mixed and so BBAOD is
27 estimated as the difference in AOD between a simulation including BB emissions and one
28 without. The total AOD from the models and from MODIS collection 5 and 6 are also shown.
29 The results show that biomass burning dominates the annual mean AOD over S. America and
30 Central to Southern Africa, even though BB emissions are highly seasonal in these regions.
31 Biomass burning also makes strong contributions to annual mean AOD in parts of Indonesia,



1 South East Asia, and Northern Australia and to a less extent the Boreal forests of N. America
2 and North East Asia. Globally BBA emissions account for 10 % of the total AOD in the
3 CLASSIC simulation and 12 % in the GLOMAP-mode simulation. The spatial distributions
4 of BBAODs are very similar in both models, which is not surprising since they are driven by
5 the same physical model and emission dataset. The magnitude of BBAODs are also very
6 similar, which again is not surprising as the emissions in each run were scaled separately to
7 match the magnitude of the AOD observations presented here and in later figures. Some
8 differences in BBAOD do occur between the two aerosol scheme due to differing
9 representation of aerosol properties and processes. Overall BBAODs are slightly higher in
10 GLOMAP-mode especially for the plume from central Africa.

11 A wider assessment of simulated AOD from GLOMAP-mode in HadGEM3 / GA7 is
12 expected in a future study but we note from Fig. 2 that GLOMAP-mode has improved the
13 distribution of AOD in several regions compared to simulation with CLASSIC. For instance,
14 it has reduced the low bias over high latitude continents (as found previously in Bellouin et
15 al., 2013) and reduced a high bias in the southern ocean associated with sea salt aerosol. The
16 AOD over the Sahara and North African Atlantic coast and Arabian Peninsula appear too low
17 in the simulations indicating that mineral dust emissions may have been too weak (in both
18 cases simulated by CLASSIC). We note however that the GLOMAP-mode simulation also
19 overestimates AOD in south-east Europe and eastern parts of USA which are dominated by
20 anthropogenic sources of sulphate. A strong caveat in these comparisons is that the modelled
21 AOD has not been sampled with the spatial and temporal incidence of the MODIS data.
22 Schutgens et al. (2015) showed that this can result in considerable regional biases between
23 modelled and observed monthly and annual mean AOD. In particular, the comparison may be
24 of limited value at high latitudes (beyond 60°N or S) where retrievals are not possible for
25 several months of the year (due to solar zenith angle being too high, or due to lack of solar
26 illumination altogether). Some degree of sampling bias may occur in regions that are
27 frequently overcast with cloud cover (e.g. marine stratocumulus regions including the South-
28 East Atlantic). The modelled AOD has however been calculated based on the clear-sky
29 relative humidity to avoid strong humidification biases in partially cloudy grid boxes.

30 **3.1.2 Seasonal AOD in biomass burning regions with MODIS**

31 Figs 3 and 4 focus on the contribution of biomass burning to AOD in the tropical regions. Fig.
32 3 shows the monthly mean BBAOD and AOD for September when BB emissions peak in the



1 Southern Hemisphere and equatorial regions. Fig. 4 shows the same for West African region
2 but for January when BB emissions peak in the zone 5 – 15° N. As in the global picture (Fig.
3 2) the simulations give very similar regional distributions of BBAOD and AOD. Overall the
4 modelled AOD in both simulations agrees very well with MODIS, especially over South
5 America and Indonesia. However, there are some discrepancies between modelled and
6 observed AODs in northern and southern parts of Africa. Firstly, the magnitude of AOD in
7 the plume over the South-East Atlantic is lower in the models than in MODIS (Fig. 3). It is
8 not clear if this is due to poor model performance or biases related to limited temporal
9 sampling by the satellite over the marine stratocumulus region (personal communication
10 Andrew Sayer). MODIS collection 5 and collection 6 in particular, show a large contrast in
11 AOD between the plume over the ocean and the AOD over adjacent land areas of Southern
12 Africa. Secondly, in Fig. 4 the peak AOD and BBAOD in the models during January are
13 centred over central Africa (Congo basin) rather than over the Gulf of Guinea where MODIS
14 AOD peaks. Again, high cloud cover limits the spatial sampling over the Congo basin and
15 may affect the mean AOD retrieved from MODIS. This regional bias was noted in previous
16 modelling studies with GFED2 (Myhre et al., 2008; Johnson et al., 2008a) and may suggest
17 there is still an underestimation in West Africa (Lioussé et al., 2012) and potentially an
18 overestimation of BB aerosol emissions in the Congo basin. The comparison of modelled and
19 observed AOD over the BB regions of the Sahel (north of 10°) is less straightforward as
20 mineral dust aerosol contributes strongly to the total AOD.

21 **3.1.3 AOD comparison with AERONET**

22 To aid the evaluation of modelled AOD, six AERONET sites have been selected representing
23 locations that are strongly affected by seasonal biomass burning. Once again, due to the
24 tuning of total BB aerosol emissions in the simulations both CLASSIC and GLOMAP-mode
25 give very similar AOD and BBAOD at these locations during peak months (Fig. 5). The
26 seasonal cycle and peak AODs seem well captured at Alta Floresta (Amazonia) and Mongu
27 (Southern Africa). The comparison at Ilorin (West Africa) shows the model does not capture
28 the observed seasonal cycle of AOD. This again suggests an under-representation of BB
29 emissions across West Africa during Northern hemisphere winter. The secondary peak during
30 June-Sept, which is not shown in the AERONET observations, may be due to overestimation
31 of BB aerosol emissions from the Congo basin and long-range transport to West Africa.
32 BBAOD appears to be underestimated at Chiang Mai (South East Asia) and Jaribu (Northern



1 Australia), perhaps by a factor of 2, but slightly overestimated at Bonanza Creek (Alaska).
2 Whilst these results give clues as to where BB aerosol emissions may be over or under
3 estimated the differences between modelled and observed AOD may be affected by various
4 other sources of uncertainty in the models and measurements. In particular, temporal
5 sampling biases may affect the results (Schutgens et al., 2015) as we have not sampled the
6 model data to match AERONET retrieval times.

7 **3.2 Aerosol composition**

8 Fig. 6a and b show the column loading of fine-mode aerosol mass from the model simulations
9 across the tropical regions during September. This is the sum of Black Carbon (BC), Organic
10 Aerosol (OA) and sulphate (SU) from all anthropogenic and natural sources but excluding the
11 coarse-mode contribution from GLOMAP. Clearly the fine-mode aerosol is dominated by BB
12 sources over Africa, South America, Indonesia and Northern Australia. Figs 6 c–h show the
13 relative contributions of OA, BC and SU to this fine-mode mass. CLASSIC and GLOMAP-
14 mode give very similar spatial distributions for the modelled fine-mode aerosol mass loading
15 and composition. OA clearly dominates the fine-mode aerosol mass (Fig. 6c and d) in both
16 models across most of the region shown, where BB emissions dominate the aerosol loading.
17 The two exceptions are the northern edge of the domain and some stretches along the Pacific
18 coast of South America where sulphates dominate due to anthropogenic emissions of SO₂. In
19 Fig 6 stipples mark grid columns where over 75 % of the fine-mode aerosol mass originates
20 from BBA emissions, based on the speciation in the CLASSIC simulation. These mark the
21 main BB plumes from S. America, Africa and Indonesia. In GLOMAP-mode where aerosols
22 internally mix the origin of the aerosol in a grid cell can not be traced to its emission source
23 but it seems reasonable to assume that the grid cells strongly influenced by BB emissions in
24 CLASSIC will also be strongly influenced by BB emissions in the GLOMAP-mode given that
25 the simulation are driven with the same emissions data and physical model configuration. The
26 similarity in the spatial distribution of BBAOD (Fig. 2 – 4) and aerosol composition (Fig. 6)
27 between the two models support this assumption. The same areas are therefore marked with
28 stipples in the GLOMAP-mode plots. The mean values beneath each plot indicate the mean
29 from the stippled areas.

30 In the main BB plumes (marked by stippling) the CLASSIC simulations show a slightly
31 higher mass fraction of OA and a slightly lower mass fraction of BC compared to GLOMAP-
32 mode with BC mass fraction averaging 5.1 % in CLASSIC and 7.2 % in GLOMAP-mode



1 (Fig. 6e and f). These differences are due to differences in the way that BB composition is
2 represented in the two schemes. In CLASSIC the ratio of BC to OA in the BBA species is
3 specified, whereas in GLOMAP-mode it varies depending on the BC and OC mass provided
4 by the emissions data, and the OC to POM ratio assumed in the model (currently 1.4). In
5 GLOMAP-mode Secondary Organic Aerosol (SOA) is also added interactively via the
6 oxidation and condensation of organic vapours from bVOCs. This decreases the BC mass
7 fraction in North Western Amazonia compared to South Eastern Amazonia and Southern
8 Africa. In CLASSIC bVOCs are not modelled explicitly but SOA has been included using a
9 biogenic aerosol climatology. This increases the OC mass, particularly over tropical forests,
10 and therefore leads to a lower BC mass fraction over tropical forests compared to Savannah
11 regions. The localized peak in BC mass fraction near to Lake Victoria in the CLASSIC
12 simulation is due to local anthropogenic BC emissions rather than BB emissions. This shows
13 up less in GLOMAP-mode as the regional loading of BC from BB sources is higher.

14 In situ measurements from three observation campaigns have been used to evaluate the
15 aerosol composition in the simulations. The observations include FAAM aircraft
16 measurements from Western Amazonia (Rondonia) and Eastern Amazonia (Tocantins) during
17 SAMBBA (Darbyshire et al., in preparation, 2016b), ground-based observations from the
18 Welgegund measurement station in South Africa (Vakkari et al. 2014), and FAAM aircraft
19 measurements from West Africa during DABEX (Capes et al. 2008). Fig. 7 compares the
20 observed and modelled aerosol composition by plotting the relative contributions from BC,
21 OA and sulphate to the total fine-mode aerosol. Nitrate, dust and sea salt have been excluded
22 from the analysis as nitrate was not available in the model simulations and accurate
23 measurements of dust and sea salt were not readily available from all observation campaigns.
24 Given that these components are neglected we can not provide a full analysis of the aerosol
25 composition here. The purpose of Fig 7 is rather to examine whether the relative proportions
26 of BC, OA and sulphate are in-line with the observational evidence (as these are the dominant
27 contributors to fine-mode mass and fine-mode AOD in the simulations).

28 In all cases the fine-mode aerosol is dominated by OA with modest contributions from
29 sulphate and generally a smaller contribution from BC. On the whole the models are able to
30 capture the typical make-up of the aerosol and some of the variations with region, such as the
31 higher contribution from sulphates in South Africa. GLOMAP-mode gives slightly higher BC
32 mass fractions than CLASSIC and in general GLOMAP-mode BC mass fractions are closer to



1 observed values. Modelling the BC mass fraction is of key importance for estimating
2 absorption and the sign of direct radiative forcing. GLOMAP-mode therefore shows some
3 improvement over CLASSIC, although it still appears to underestimate BC mass fraction
4 relative to the measurements from West Africa, Eastern Amazonia, and to a lesser extent in
5 South Africa. However, the use of the filter based absorption measurements in those datasets
6 may lead to a significant overestimation of observed BC mass (Lack et al., 2008). Also, note
7 that different mass absorption coefficients were assumed in the analyses of the DABEX
8 ($12\text{m}^2/\text{g}$) and Welgegund ($6.6\text{m}^2/\text{g}$) observations. Unifying this assumption to an
9 intermediate value of $10\text{m}^2/\text{g}$ would change the estimated BC mass fraction to 14.1 % for
10 DABEX and 8.2 % for Welgegund.

11 3.3 Size distributions

12 3.3.1 Comparison with aircraft data

13 Fig. 8 shows the size distributions from the models and in situ observations from the three
14 aircraft campaigns. The CLASSIC curve is simply the size distribution given by the average
15 mixture of fresh and aged BBA species in the model. Each of these CLASSIC modes is
16 represented by a single log-normal. Both modes have a small standard deviation of 1.3 and
17 the mean diameters are $0.2\ \mu\text{m}$ for the fresh mode and $0.24\ \mu\text{m}$ for the aged mode. Combining
18 these gives a fairly narrow distribution peaking in the accumulation mode. The GLOMAP-
19 mode size distribution is the sum of all five modes (nucleation, Aitken soluble and insoluble,
20 accumulation soluble, coarse soluble). Each campaign includes data from a common PCASP
21 instrument but SAMBBA included a GRIMM OPC behind a low-turbulence inlet and a
22 Scanning Mobility Particle Sizer (SMPS). These instruments provide a dry aerosol size
23 distribution as heating tends to remove water from the measured aerosol samples. The
24 three instruments from SAMBBA are in good agreement regarding the shape of the
25 accumulation mode and the rate of decline from the accumulation to coarse mode ($0.3 -$
26 $1\ \mu\text{m}$). To avoid mismatches from sampling different total concentrations, the PCASP size
27 distributions have been normalized to give a total concentration of unity, and other observed
28 and modelled curves have been normalized to match the peak amplitude of the PCASP.

29 The dry particle size distribution simulated by GLOMAP-mode is shown in Fig. 8 and
30 matches the observed size distributions remarkably well. The broad peak in aerosol number
31 around $0.2\ \mu\text{m}$ and the rate of decline either side of the peak seem well supported by the



1 available observations. The discrepancies between the GLOMAP-mode and observed size
2 distributions across the coarse mode ($D > 1\mu\text{m}$) are most likely because mineral dust is not
3 represented in this version of the modal scheme (this is certainly the reason in the DABEX
4 case; Fig. 8b). Another potential issue in the Amazon case is the absence in the model of any
5 representation of primary biological aerosol particles which may contribute significantly to
6 the observed coarse mode in this forested region (e.g. Scot et al., 2012), though such particles
7 are only likely to be important in the surface mixed layer. Also, measurements of low
8 concentrations of super-micron particles will have bigger uncertainties than measurements of
9 the accumulation-mode peaks. The agreement between GLOMAP-mode and the observations
10 across the accumulation mode ($0.1 - 0.6\mu\text{m}$) is partly due to a well chosen initial size
11 distribution that is assumed for primary emissions of BBA (this a log-normal with a mean
12 diameter of $0.15\mu\text{m}$ and standard deviation of 1.59 as used by Stier et al., 2005). This sets the
13 mass and number of particles emitted into the Aitken insoluble mode. Subsequently, as a
14 result of ageing these particles grow and are transferred to the accumulation soluble mode,
15 where most of the BC and OA mass ultimately resides. Here coagulation and condensation
16 create an internal mixture of sulphate, sea salt, OC, BC and water from all modelled sources.
17 The combination of a well chosen initial size distribution for the primary emissions, and
18 subsequent microphysical and chemical processes operating through the modal framework,
19 are therefore very successful in predicting the aerosol size distribution over BB regions.

20 CLASSIC provides a reasonable representation of the aerosol size distribution through the
21 centre of the accumulation mode ($0.1 - 0.6\mu\text{m}$) that is most important for optical properties in
22 the visible and near-infrared spectrum. CLASSIC naturally fits the SAFARI-2000 PCASP
23 observations (Fig. 8c), on which it was originally based (Haywood et al. 2003), but also fits
24 the DABEX and SAMBBA observations reasonably well across the intended size range.

25 It is interesting to note that the observed size distributions do not vary greatly across the
26 accumulation mode ($0.1 - 0.6\mu\text{m}$) between the three BB campaigns. These campaigns span
27 three of the main continental source regions of BBA (Fig. 9a) and include a range of biomes
28 and fire conditions. This finding of little variation in size distribution between different
29 biomass burning source regions suggests the approach of using a globally representative size
30 distribution in CLASSIC, and of using a single “emission size distribution” for all primary
31 biomass burning emissions in GLOMAP-mode is a reasonable approximation. We note
32 however that Dentener et al. (2006) present a synthesis of observations from a wider



1 collection of observations, suggesting considerable variation in size distribution (their Figs.
2 C1 and C2). These indicate apparently large changes in physical and optical properties
3 between different biomass burning source regions and/or following ageing of plumes. The
4 large differences shown in Dentener et al. (2006) could in part be related to differences in
5 systematic biases or sizing corrections applied to differences instruments, while here we
6 present coherent results from essentially the same instrument (Fig 9b).

7 **3.3.2 Comparison with AERONET size distributions**

8 In Fig. 10 AERONET retrievals of particle size distribution are used as an additional
9 constraint to assess the modelled aerosol size distribution. These are given in terms of particle
10 volume across the fine and coarse modes (0.1 – 15 μm) and all distributions have been
11 normalized to give peak amplitudes of 1. The overall shape of the distribution varies very
12 little from year to year (Fig 10a) with a dominant fine-mode peaking around 0.3 μm . The
13 relative contribution from coarse-mode particles varies from year to year but is generally
14 small. A similar analysis was performed for Mongu and produced an almost identical fine-
15 mode size distribution giving some confidence that Alta Floresta is representative for tropical
16 biomass burning regions.

17 Fig. 10b compares the AERONET size distribution to the PCASP and GRIMM OPC aircraft
18 instrument data from the Western SAMBBA region. Again, all size distributions have been
19 normalized to give the same peak amplitude. It is encouraging that the PCASP gives an
20 almost identical size distribution to AERONET across the fine-mode. The GRIMM OPC size
21 distribution covers only a portion of the fine-mode size range but the data are consistent with
22 the existence of a peak at 0.3 μm , a minimum around 1 μm and a peak at coarser sizes. The
23 aircraft instruments do not agree so well with AERONET on the amplitude or diameter of the
24 coarse mode. The coarse-mode could be a mixture of mineral dust, primary biogenic particles
25 or fly ash from BB (Martin et al., 2010). Sampling issues may be a large source of error in the
26 PCASP and GRIMM measurements of super micron particles. However, the coarse-mode is
27 not the focus of the assessment here as the sources are unclear and it contributes very little (5
28 – 10 %) to the AOD or optical properties.

29 Fig. 10c compares the mean AERONET size distribution with the models. For CLASSIC the
30 size distribution of the BBA species is plotted whereas GLOMAP-mode is the column-mean
31 for September co-located with Alta Floresta. Both modelled size distributions peak at about
32 the same diameter (~0.3 μm) as AERONET. The CLASSIC size distribution is a little



1 narrower than AERONET whereas GLOMAP-mode predicts about the same width as
2 AERONET. This increases confidence that GLOMAP-mode is able to predict aerosol size
3 distributions accurately, and is an improvement over the specified distribution in CLASSIC.

4 **3.4 Optical properties**

5 In this section the aerosol optical properties from the models are compared and evaluated
6 against AERONET retrievals and in-situ measurements from aircraft campaigns. The methods
7 for deriving optical properties are described below and results are then discussed separately
8 for each optical property.

9 Firstly the column-average moist aerosol properties have been calculated from the models to
10 assess how these vary regionally in the two aerosol schemes. The fine-mode specific
11 extinction coefficient ($k_{\text{ext, fm}}$) (Fig. 11a & b) was calculated as the ratio of fine-mode moist
12 AOD to fine-mode dry aerosol mass. In GLOMAP-mode the fine-mode includes the Aitken
13 soluble, Aitken insoluble and accumulation-soluble modes. In CLASSIC the fine-mode is
14 taken to include all sulphate and carbonaceous aerosol species. The Single Scattering Albedo
15 (SSA) (Fig. 11c & d) has been calculated from the AOD and Absorption-AOD (AAOD) at
16 550nm, and the Ångström exponent (Å) (Fig. 11e & f) is calculated from the wavelength
17 dependence of AOD across 440 – 670nm. The stipples in Fig. 11 mark grid columns where
18 over 75 % of the fine-mode aerosol mass originates from BBA emissions (as in Fig. 6, based
19 on CLASSIC speciation) and the mean values beneath each plot indicate the mean from the
20 stippled areas.

21 Secondly, the modelled SSA and Å are compared for all months against AERONET retrievals
22 for Alta Floresta and Mongu (Fig. 12). Monthly mean SSA retrievals were not available in all
23 months of the year due to low temporal sampling frequency outside of the dry season
24 (inversions require AOD > 0.4 and cloud-free skies). In addition to AERONET level 2 criteria
25 we only accept a monthly mean if data were available from at least 3 separate days in that
26 month, and only calculate the long-term monthly mean if at least 3 monthly means were
27 available in the time series. The AERONET retrievals of Å relied on direct sun measurements
28 of AOD at 440 and 670nm and have better temporal sampling enabling long-term monthly
29 means to be calculated for every month.

30 Finally, Table 2 compares dry aerosol optical properties of SSA, Å , $k_{\text{ext, fm}}$, and asymmetry
31 parameter (g) from the models and from the mean values from the aircraft campaigns



1 (references provided in the table). The comparison is made for dry aerosol since heating tends
2 to dry the aerosol samples measured by the aircraft instruments. For CLASSIC, the optical
3 properties are specified and so values in Table 2 are simply derived by averaging together the
4 optical properties for fresh and aged BBA species, based on the typical mixture simulated
5 over the BB regions (10 % fresh, 90 % aged). For GLOMAP-mode the dry optical properties
6 in Table 2 were calculated from Mie theory using the dry size distribution and refractive
7 index for each of the fine modes (Aitken soluble, Aitken insoluble and accumulation-soluble)
8 and then averaged across the modes weighting by total extinction (or by scattering for g).

9 **3.4.1 Fine-mode specific extinction coefficient ($k_{\text{ext, fm}}$)**

10 The fine-mode moist specific extinction (Fig. 11a & b) varied quite widely in both models but
11 was generally higher in GLOMAP-mode, especially in areas where sulphates were more
12 dominant (see Fig. 6h). This is due to a high water uptake by sulphate in the current
13 GLOMAP-mode configuration. In the main BB plumes (marked by stipples), where OA
14 dominates the aerosol mass, the values of $k_{\text{ext, fm}}$ range from 5 – 10 m^2/g with the highest
15 values in both models over the moister regions of Indonesia and the lowest values in Southern
16 Africa where the average relative humidity was lower in the lower troposphere (not shown).
17 The average values from the BB plumes (stippled areas) are fairly similar with slightly lower
18 value of 6.2 m^2/g for CLASSIC and a value of 6.9 m^2/g for GLOMAP-mode. Note these
19 values are indicative of the aerosol mixture as a whole rather and so are affected by the
20 representation of other aerosols also. In Table 2 the dry values of $k_{\text{ext, fm}}$ are similar for
21 CLASSIC (5.0 m^2/g) and GLOMAP-mode (4.5 – 4.8 m^2/g) and are within the range given by
22 the aircraft measurement campaigns (3.6 – 5.8 m^2/g). Note, in this case the dry value given for
23 CLASSIC corresponds to the BB species only.

24 **3.4.2 Single scattering albedo (SSA)**

25 The SSA of aerosol over BB dominated regions was generally lower in GLOMAP-mode than
26 in CLASSIC for both the ambient (moist) values (Fig. 11c and d; Fig. 12a and c) and dry
27 values (Table 2). This is consistent with the higher BC mass fraction in GLOMAP-mode (Fig
28 7). The lower dry SSA values from GLOMAP-mode (0.85 – 0.87) agree better with the range
29 from the aircraft campaigns (0.79 – 0.88) than CLASSIC (0.91). The ambient SSA values
30 from GLOMAP-mode during the dry season (July – Oct) (0.87 – 0.94) also agree better with
31 AERONET observations from Alta Floresta and Mongu (Fig. 12a and c). The ambient SSA



1 also shows a high degree of spatial variability in both models (Fig. 11c and d). These
2 variations are mainly caused by variability of composition and water content. As shown in
3 section 3.5 the hygroscopic growth may be overestimated in both models so the spatial
4 variation of ambient SSA and its relation to humidity may not be entirely realistic. However,
5 the AERONET observations do show a contrast between the drier region of Southern Africa
6 (represented by the Mongu site in Fig. 11c) where the long-term monthly mean SSA drops to
7 0.82 – 0.85 during July – September, and the moister Amazonian region (represented by the
8 Alta Floresta site in Fig. 11a) where the long-term monthly SSA is around 0.92 during August
9 – September. This observed variation may be explained more by variations in BC content
10 rather than due to variations in hygroscopic growth. There is likely a higher BC content in the
11 aerosol column over Mongu due to the drier vegetation burning more through flaming
12 combustion (some evidence for the higher BC content is found in Fig. 7d for the Welgegend
13 observations that are in the same continental region).

14 **3.4.3 Ångström exponent (\AA)**

15 The CLASSIC aerosol scheme gives a fairly high Ångström exponent with a dry value of 2.3
16 for the BBA species (Table 2), and moist values of 1.9 – 2.1 for the fine-mode aerosol
17 mixture over BB dominated regions (Fig. 11e). This is due to the fairly narrow size
18 distribution assumed in CLASSIC. These values of \AA are somewhat outside the observed
19 range from the aircraft campaigns (dry values of 1.7 – 2.1 from nephelometer measurements)
20 and AERONET (long-term monthly mean moist values of 1.7 – 1.9). GLOMAP-mode gives
21 slightly lower values of \AA than CLASSIC, with dry values ranging from 2.0 – 2.1 (Table 2),
22 and ambient (moist) values ranging from 1.5 – 1.9 over the BB regions (Fig. 11f). These agree
23 quite well with the aircraft observations and AERONET observations during the peak of the
24 burning season (Aug-Sept) (Fig. 12b and d). The seasonal variation of \AA observed by
25 AERONET (i.e. the drop to lower values outside the burning season in Fig. 12b & d) is not
26 well captured in either model. This could be due to insufficient representation of coarse
27 particles, such as mineral dust or primary organic particles outside the BB season.

28 **3.5 Hygroscopic growth**

29 The hygroscopic growth of aerosol (i.e. the growth of the aerosol with relative humidity due
30 to the uptake of water) leads to enhanced scattering. This can be expressed via the Scattering
31 Growth Factor (GF_{sea}), which is the observed or modelled scattering of the aerosol at ambient



1 humidity divided by the scattering of the same aerosol when completely dried (i.e. at very low
2 relative humidity). For CLASSIC the hygroscopic growth is specified via an empirical fit that
3 reproduces the GF_{sca} curve observed by Magi and Hobbs (2003), hereafter MH03. In MH03
4 GF_{sca} curves were derived from a humidified nephelometer system operated on flights over
5 Southern Africa during SAFARI-2000. MH03 parameterized the GF_{sca} curves for a range of
6 aerosol conditions and the CLASSIC scheme uses their “heavy smoke” curve for the fresh
7 BBA species, and their “regional air” curve for the aged BBA species. These GF_{sca} curves are
8 shown on Fig 13, along with a representative curve for CLASSIC assuming a mixture with 10
9 % fresh BBA and 90 % aged BBA. These give a very strong increase of scattering with RH
10 for the CLASSIC BBA, with GF_{sca} rising to 2.05 at 80 % and to 3.4 at 100 %. With similar
11 instrumentation Kotchenruther and Hobbs (1998), hereafter KH98, found much lower GF_{sca}
12 for BB dominated aerosol over Brazil (Fig. 13). For $RH > 65$ % the range from KH98 does
13 not overlap that from MH03, and at 80 % the range from KH98 is only 1.05 – 1.29. The large
14 difference between these two observation sets is difficult to reconcile, especially as both were
15 derived from an airborne humidified nephelometer system. Possibly the regional aerosol
16 mixture (categorised as “regional air” in MH03) contained a substantial proportion of highly
17 hygroscopic sulphate from industrial sources in Southern Africa and is therefore not
18 representative of purely carbonaceous aerosol.

19 Additional constraints on hygroscopic growth have been provided more recently from
20 Hygroscopic Tandem Differential Mobility Analyzer (H-TDMA) instruments. A wide range
21 of measurements, including Amazonian aerosol are summarized in the review of Swietlicki et
22 al. (2008). More recent measurements for Amazonia are also provided in Whitehead et al.
23 (2014). In these analyses the hygroscopic growth is summarized via the “kappa” parameter
24 (κ) that can be used to reconstruct the growth curve from Kohler theory. Swietlicki et al.
25 (2008) give a range of κ values of 0.05 – 0.15 for Amazonian dry season / BB conditions,
26 leading to GF_{sca} of 1.16 – 1.49 at 80 %. The Kohler curves based on this range of κ are also
27 plotted in Fig. 13. For $RH < 90$ % the Kohler curves provide an intermediate range of growth
28 factors that overlap the upper range from KH98 and the lower range from MH03. However,
29 the Kohler curves have greater curvature and rise very steeply for $RH > 80$ % and exceed the
30 range from MH03 for $RH > 95$ %. This reflects the increasing level of uncertainty in GF_{sca} at
31 higher RH where growth factors become increasingly difficult to verify from the
32 observations. Both the empirical fits in KH98 and MH03, and the theoretical Kohler curves
33 are essentially extrapolated from the observed growth up to 80 % or 90 %.



1 For GLOMAP-mode the hygroscopic growth curve is calculated based on the Zdanovski-
2 Stokes–Robinson (ZSR; Stokes and Robinson, 1966) mixing rule. For this comparison we
3 take the average fine-mode composition from the four regions / sites in Fig 7, which gives a
4 mixture with 82.6 % organic carbon, 9.4 % sulphate, and 8 % black carbon. The black carbon
5 is assumed to be hydrophobic whereas organic carbon is assumed hydrophobic when in the
6 Aitken insoluble mode (where approximately one third of the OA resides) and hygroscopic in
7 the soluble modes (most of the remaining two-thirds of OA). The water uptake by soluble OA
8 is based on sulphuric acid but scaled down such that the carbonaceous aerosol from BB takes
9 up approximately 25 % of the water of an equivalent dry mass of H₂SO₄. The GF_{sca} curve in
10 GLOMAP-mode is capped at a RH of 90 % to avoid overestimation of aerosol scattering and
11 AODs close to saturation. For relative humidity above 60 % GLOMAP-mode gives lower
12 GF_{sca} than CLASSIC, with GF_{sca} reaching 1.66 at 80 % and 2.19 for 90-100 % (compared to
13 2.1 and 2.6 – 3.4 for CLASSIC). For RH < 60 % GLOMAP-mode has a slightly higher GF_{sca}
14 than CLASSIC and has an unrealistic shape, but this is unlikely to be important compared to
15 the difference at higher RH.

16 Overall, although there is large uncertainty from the observations it seems likely that the
17 CLASSIC scheme overestimates the GF_{sca} and therefore aerosol scattering, AOD and single
18 scattering albedo for BBA in moist conditions (e.g. RH > 60 %). GLOMAP-mode may also
19 overestimate the hygroscopic growth, though to a lesser extent. The representation of
20 hygroscopic growth could be improved in both aerosol schemes. One option would be to use
21 Kohler curves with observationally constrained κ values, though care would be needed in
22 dealing with the growth assumed at the upper RH range.

23 3.6 Vertical distribution of aerosol

24 The vertical distribution of BBA in the models depends on the vertical profile of emissions
25 and on transport and removal processes. The emission profiles and transport processes are
26 treated identically for the two aerosol schemes but the representation of wet and dry removal
27 processes are different. The modelled profiles of fine-mode aerosol mass are assessed in Fig.
28 14 by comparing them with campaign-mean aircraft observations. For the SAMBBA and
29 DABEX cases the observed profile of fine-mode mass has been estimated from the
30 nephelometer measurement of dry aerosol scattering multiplied by the fine-mode specific
31 extinction ($k_{\text{ext, fm}}$) and SSA. Due to use of a modified Rosemount inlet serving the
32 nephelometer on the FAAM aircraft, coarse-mode particles are not well sampled. We



1 therefore make the assumption that the total nephelometer scattering serves as a reasonable
2 guide to fine-mode aerosol concentration. For the conversion of scattering to fine-mode mass
3 we take the $k_{\text{ext, fm}}$ and SSA values derived from the in-situ aircraft observations in Table 2.
4 For SAMBBA (Fig. 14a) the campaign mean profile is representative of the Western
5 Amazonia region around Porto Velho, Rondonia. The aerosol extinction coefficient derived
6 from the airborne lidar in SAMBBA was also averaged over a range of flights observing
7 regional BBA layers in the Amazonian region (Marenco et al., 2015). The lidar-derived
8 extinction at 355nm was converted to dry extinction at 550nm using an Ångström exponent of
9 1.7 based on the AERONET September monthly mean at Alta Floresta (Fig. 12a), and the
10 average humidity growth factor from KH98 (Fig. 13). For DABEX the campaign mean
11 profile is taken from Johnson et al. (2008a) and included a correction to subtract the scattering
12 associated with mineral dust aerosol. For SAFARI-2000 no campaign mean profile was
13 available but Haywood et al. (2003) provides information on the observed range of heights for
14 the elevated layers observed over the South East Atlantic. To indicate the degree of sampling
15 error in the mean profiles the standard error is also shown in Fig. 14 for both the observations
16 and models. For the observations the standard error has been calculated as the standard
17 deviation of aerosol mass at a given altitude divided by the square root of the number of
18 profiles (for the nephelometer) or flight sections (for the lidar). For the models the standard
19 error is calculated as the standard deviation from the ten monthly mean profiles in each
20 simulations, divided by the square root of ten (the number of years).

21 The two models predict very similar vertical distributions of fine-mode aerosol with
22 approximately the same profile shape and magnitude of aerosol mass. In most places
23 differences between the models are comparable to the standard error associated with
24 interannual variability. The models also agree quite well with the observations in terms of
25 reproducing the basic vertical structure and profile shape. Over Amazonia the observed
26 profile shows a fairly well mixed layer up to 1.5km, a small increase around 1.5- 2 km and
27 then a gradual decline from 2 – 6 km and very little above 6km. The lidar gives a similar
28 shaped profile to the nephelometer except with a more pronounced peak around 2km.
29 Although the concentrations of aerosol mass observed during SAMBBA were highly variable
30 in space and time (Marenco et al., 2016), the relatively low standard error shows that by
31 averaging over a sufficient sample of flight sections (lidar) or profiles (nephelometer) the
32 campaign mean nephelometer and lidar profiles do provide a useful guide for evaluating the
33 models. The lidar and nephelometer profiles are not expected to match exactly as the spatial



1 and temporal sampling frequency was different and lidar profiles are more uncertain near the
2 ground. Both models capture the shape of the observed profiles reasonably well even showing
3 the increase around 2km. During DABEX the BB dominated aerosol layers were observed to
4 reside in an elevated layer from 1.5 – 5 km with only low concentrations below. These
5 elevated layers originated from BB emissions further south but had been undercut by Saharan
6 air, lofted and transported north and west towards the observed region (mainly around
7 Niamey, Niger). The models capture the elevated layer but predicted concentrations are lower
8 than observed. During SAFARI-2000 the BB dominated aerosol over the South Eastern
9 Atlantic were observed to reside in elevated layers with a fairly consistent layer base at 1.5 +/-
10 0.6 km and layer top at 4.9 +/- 0.7km. The models both simulate an elevated layer peaking
11 within this altitude range but with some spread above and below the observed limits of the
12 layers. The two models give very similar vertical profiles though the mass concentration
13 peaks at slightly higher values in CLASSIC in the centre of the layer.

14 Overall the results show that HadGEM3 predicts the vertical profile of BBA quite well
15 despite the current rather crude set of assumptions for plume injection height. As detailed in
16 section 2.3 the emissions from Savannah were injected at the surface and emissions from
17 forest/deforestation uniformly over the lowest 3km. More sophisticated approaches where
18 plume injection heights are predicted online in the model should certainly be investigated, but
19 it is encouraging that the current approach works reasonably well for the cases investigated
20 here.

21 **4 Conclusions**

22 We conclude that the implementation of GLOMAP-mode has improved the representation of
23 biomass burning aerosol in HadGEM3. The modal scheme is able to predict the full aerosol
24 size distribution, and simulate the variation of aerosol composition and optical properties
25 giving the scheme increased accuracy over the CLASSIC bulk scheme of HadGEM2-ES. The
26 simulated aerosol properties, AOD and aerosol vertical distribution are shown to compare
27 well with observations from SAMBBA and two other aircraft campaigns (DABEX, SAFARI-
28 2000), and with remote sensing retrievals from MODIS and AERONET.

29 The analysis of field observations showed biomass burning aerosols to have reasonably
30 consistent size distributions, Ångström exponents (1.7 – 2.1) and dry specific extinction
31 coefficients (3.6 – 5.8 m²/g) across different tropical biomass burning regions. CLASSIC
32 represents this reasonably well by specifying a globally-representative size distribution that



1 includes the particle size range most important for interaction with solar radiation. GLOMAP-
2 mode simulated the full size distribution from nucleation to coarse (0.01-10 μ m), showing
3 realistic features with good agreement against the available observations. The agreement
4 between modelled and observed size distributions stems from a well constrained initial size
5 distribution for the emitted particles, followed by a good representation of how this size
6 distribution evolves with chemical and microphysical processes. GLOMAP-mode was also
7 able to predict the optical properties with improved accuracy.

8 However, the analyses suggest that both aerosol schemes overestimate the uptake of water at
9 high relative humidity. This overestimation is greater in CLASSIC and is likely to cause an
10 overestimation of aerosol scattering, AOD and SSA in moist regions. In CLASSIC the aerosol
11 scattering coefficient rises by a factor of 2.1 from dry conditions to 80 % relative humidity,
12 whereas in GLOMAP-mode it rises by a factor of 1.7. Although there is considerable
13 uncertainty and variability amongst observations, recent measurement from H-TDMA
14 suggest lower growth factors for aged BB aerosol with the factor of increase in aerosol
15 scattering in the region of 1.2 – 1.5 from dry to 80 % relative humidity.

16 The analysis of observations in this study also highlights the strong variations in black carbon
17 (BC) mass fraction (5 – 12 %) and Single Scattering Albedo (SSA) (0.79 – 0.88) in the
18 average biomass burning aerosol composition from different tropical source regions. These
19 variations are a challenge for the models to capture. Whilst the dry BC mass fraction and SSA
20 in GLOMAP-mode (7-10 %; 0.85 – 0.87) are closer to the observed values than CLASSIC (5-
21 9 %; 0.91), the variability between source regions is lower than observed. This may point to
22 the need for a wider range of BC:OC ratios in the emissions data, which in GFED3 are based
23 on Andreae and Merlet (2001). These have been updated in GFED4 (Giglio et al., 2013)
24 based on Akagi et al. (2011) and future studies may provide useful feedback on whether these
25 improve the variability of aerosol composition in models. The emissions of BBA had the
26 same prescribed vertical profile in both models and led to very similar vertical distributions of
27 fine-mode aerosol mass over the main tropical BB regions that compared well with the
28 airborne in-situ and lidar observations.

29 Whilst both schemes gave good agreement between observed and modelled AODs over BB
30 regions, this was achieved by scaling up the total aerosol emissions from GFED3.1 by a
31 global scaling factor of 1.6 for CLASSIC and 2.0 for GLOMAP-mode. This might suggest
32 that the emissions of BC and OC from GFED3 lead to an underestimate of the aerosol mass.



1 However, we note that there is considerable uncertainty in other parameters in the models that
2 affect the aerosol mass and AOD from BB sources. Firstly, there is considerable uncertainty
3 in the ratio used to convert the OC (i.e. carbon mass provided by the emissions data) to the
4 total mass of POM emitted in the models. This depends on the ratio of carbon to oxygen and
5 other elements in the emitted aerosol. In the current configuration of HadGEM3 CLASSIC
6 does not account for this issue (effectively neglecting the non-carbon mass) and GLOMAP-
7 mode converts the OC to POM using a ratio of 1.4 that is likely too low for biomass burning
8 emissions. On the other hand CLASSIC increases the total aerosol mass by a factor of 1.62 on
9 a 6 hour e-folding timescale to represent condensation growth during ageing (a process that
10 GLOMAP-mode does not include). Therefore, the emission scaling factors required to
11 generate agreement between modelled and observed AODs clearly depend on these other
12 scaling applied within the aerosol schemes, as well as aerosol optical properties and aerosol
13 lifetime. Other models may not require emission scaling to gain good agreement with
14 observed AODs or may require different scaling factors outside the range 1.6 – 2.0 found in
15 this study. It is also worth noting that there are large differences between emission factors
16 estimated for difference measures of the aerosol mass: BC + OC, Total Carbon (TC), Total
17 Particulate Matter (TPM), PM_{2.5} and PM₁₀ (see Andreae and Merlet 2001; Akagi et al.,
18 2011). For instance the emission factors for TPM are a factor of 2.3 – 2.4 higher than the sum
19 of BC + OC in GFED3 (based on Andreae and Merlet 2001) for tropical BB sectors. Using
20 TPM instead of BC and OC in our simulations would therefore have led to an overestimation
21 of AOD in tropical regions unless the global emission scaling factor was reduced to
22 approximately 0.67 in CLASSIC and approximately 1.15 in GLOMAP-mode. With such large
23 uncertainty and observed variability in emission factors, POM:OC ratios, hygroscopic growth
24 and secondary formation of organics, it is difficult to advocate any particular set of changes
25 that would improve the models, though clearly there is scope to reduce the discrepancy
26 between modelled and observed AOD without the use global emission scaling factors.

27 Furthermore, although tuning the emissions gave good overall agreement with observed AOD
28 in the dominant tropical BB regions, some regional discrepancies remained. In particular, we
29 note a low bias over West Africa and a high bias over the Congo basin during Northern
30 hemisphere winter. The AOD over South East Asia and Northern Australia during their BB
31 seasons were also underestimated in our simulations, but the contribution of BB to AOD in
32 the high latitude Boreal forests seems to be slightly overestimated. Regional biases in AOD
33 may be caused, to some extent, by regional (or biome specific) biases in the total emission



1 rate. Other factors may include variations in aerosol optical properties between different
2 regions (e.g. due to different size distribution or water uptake) that may not be captured in the
3 models. Applying a globally uniform scaling factor to account for current uncertainties in BB
4 emission datasets is therefore not sufficient to reconcile the modelled AOD with observations.
5 GFED version 4 (Giglio et al., 2013) has already made significant progress in addressing
6 biases related to small fires (Randerson et al., 2012) that are difficult to identify from burned
7 area products. Follow on studies from this work are recommended to assess the impact of
8 recent developments in fire emission modelling on reducing such regional biases.

9 Overall we conclude that GLOMAP-mode provides a good simulation of BB aerosol for
10 modelling their impacts on radiation and climate. Impacts on CCN and cloud microphysics
11 have not been evaluated here but have been assessed previously in Bellouin et al. (2013). This
12 study does show clear improvements to the aerosol size distribution and composition in
13 GLOMAP-mode that is important for aerosol indirect effects. This shows the benefits of
14 including a more detailed representation of aerosol microphysical and chemistry processes.
15 However, the model could merit from further improvements to BB processes, including more
16 accurate estimates of the emission flux, the composition of emitted particles (which can vary
17 considerably with vegetation / fuel type), and the injection height profile. We also note large
18 uncertainties in the representation of hygroscopic growth, ageing, and absorption (including
19 the role of brown carbon). This is partly due to the complexity of these processes and
20 difficulties in constraining them with observations.

21 **Author contributions**

22 J. Langridge, E. Darbyshire, W. Morgan, K. Szpeck, J. Brooke, F. Marengo contributed
23 towards the analysis of FAAM aircraft observations from SAMBBA, J. Haywood, H. Coe, P.
24 Artaxo, K. Longo were co-principal investigators on the SAMBBA project, J. Mulcahy, G.
25 Mann, N. Bellouin, M. Dalvi contributed to the implementation of GLOMAP-mode aerosol
26 scheme in HadGEM3.

27

28 **Acknowledgements**

29 The Facility for Airborne Atmospheric Measurement (FAAM) BAe-146 Atmospheric
30 Research Aircraft is jointly funded by the Met Office and Natural Environment Research
31 Council and operated by DirectFlight Ltd. We would like to thank the dedicated efforts of



1 FAAM, DirectFlight, INPE, University of Sao Paulo, and the Brazilian Ministry of Science
2 and Technology in making the SAMBBA measurement campaign possible. For AERONET
3 data we thank the PI investigators and their staff for establishing and maintaining the sites
4 used in this investigation (Alta Floresta and Mongu: Brent Holben, Ilorin: Rachel T. Pinker,
5 Chiang Mai: Serm Janjai, Bonanza Creek: John R. Van de Castle, Jabiru: Ross Mitchell). We
6 thank Andrew Sayer and Robert Levy from Goddard Space Flight Centre for their advice with
7 MODIS aerosol products. We thank Ville Vakkari for help in selecting data from the
8 Welgegund station. JMH, ED, WTM, HC, GM and NB were funded by SAMBBA (NERC
9 grant NE/J009822/1). BJ, JMH and JM were funded under the Joint UK DECC/DEFRA –
10 Met Office Hadley Centre Climate Programme (GA01101). JMH was part funded by the
11 IMPALA grant (NE/M017214/1) via Future Climates for Africa (FCA) funding provided by
12 NERC and DFID.

13 **References**

- 14 Abel, S. J., Haywood, J. M., Highwood, E. J., Li, J., and Buseck, P. R.: Evolution of biomass
15 burning aerosol properties from an agricultural fire in southern Africa., *Geophys. Res.*
16 *Lett.*, 530, 1783, 2003.
- 17 Akagi, S. K., Yokelson, R. J., Wiedinmyer, C., Alvarado, M. J., Reid, J. S., Karl, T., Crouse,
18 J. D., and Wennberg, P. O.: Emission factors for open and domestic biomass burning for use
19 in atmospheric models, *Atmos. Chem. Phys.*, 11, 4039–4072, doi:10.5194/acp-11-4039-2011,
20 2011.
- 21 Aiken, A. C., DeCarlo, P. F., Kroll, J. H., Worsnop, D. R., Huffman, J. A., Docherty, K.,
22 Ulbrich, I. M., Mohr, C., Kimmel, J. R., Sueper, D., Sun, Y., Zhang, Q., Trimborn, A.,
23 Northway, M., Ziemann, P. J., Canagaratna, M. R., Onasch, T. B., Alfarra, M. R., Prevot,
24 A. S. H., Dommen, J., Duplissy, J., Metzger, A., Baltensperger, U., and Jiménez, J. L.:
25 O/C and OM/OC Ratios of Primary, Secondary, and Ambient Organic Aerosols with a
26 High Resolution Time-of-Flight Aerosol Mass Spectrometer, *Environ. Sci. Technol.*, 42,
27 4478–4485, 2008.
- 28 Allan, J. D., Morgan, W. T., Darbyshire, E., Flynn, M. J., Williams, P. I., Oram, D. E.,
29 Artaxo, P., Brito, J., Lee, J. D., and Coe, H.: Airborne observations of IEPOX-derived
30 isoprene SOA in the Amazon during SAMBBA, *Atmos. Chem. Phys.*, 14, 11393–11407,
31 doi:10.5194/acp-14-11393-2014, 2014.



- 1 Andreae, M. O., Merlet, P.: Emission of trace gases and aerosols from biomass burning,
2 Glob. Biogeochem. Cycles, 15, Issue 4, 955-966, 2001.
- 3 Andreae, M. O., Rosenfeld, D., Artaxo, P., Costa, A. A., Frank, G. P., Longo, K. M., and
4 Silva-Dias, M. A. F.: Smoking rain clouds over the Amazon, Science, 303, 1337–1342,
5 doi:10.1126/science.1092779, 2004.
- 6 Andres, R. J. and Kasgnoc, A. D.: A time-averaged inventory of subaerial volcanic sulfur
7 emissions, J. Geophys. Res., 103, 25 251–25 261, 1998.
- 8 Andrews, E., Sheridan, P., Fiebig, M., McComiskey, A., et al.: Comparison of methods
9 for deriving aerosol asymmetry parameter, J. Geophys. Res., 111, D05S04,
10 doi:10.1029/2004JD005734, 2006.
- 11 Archer-Nicholls, S., Lowe, D., Schultz, D. M., and McFiggans, G.: Aerosol–radiation–cloud
12 interactions in a regional coupled model: the effects of convective parameterisation and
13 resolution, Atmos. Chem. Phys., 16, 5573-5594, doi:10.5194/acp-16-5573-2016, 2016.
- 14 Bauer, S. E., and Menon S.: Aerosol direct, indirect, semidirect, and surface albedo effects
15 from sector contributions based on the IPCC AR5 emissions for preindustrial and present-day
16 conditions, J. Geophys. Res., 117, D01206, doi:10.1029/2011JD016816.
- 17 Bellouin, N., Mann, G. W., Woodhouse, M. T., Johnson, C., Carslaw, K. S., and Dalvi, M.:
18 Impact of the modal aerosol scheme GLOMAP-mode on aerosol forcing in the Hadley Centre
19 Global Environmental Model, Atmos. Chem. Phys., 13, 3027-3044, doi:10.5194/acp-13-
20 3027-2013, 2013.
- 21 Bellouin, N., Rae, J., Jones, A., Johnson, C., Haywood, J., and
22 Boucher, O.: Aerosol forcing in the Climate Model Intercomparison Project (CMIP5)
23 simulations by HadGEM2-ES and the role of ammonium nitrate, J. Geophys. Res., 116,
24 D20206, doi:10.1029/2011JD016074, 2011.
- 25 Brito, J., Rizzo, L. V., Morgan, W. T., Coe, H., Johnson, B., Haywood, J., Longo, K., Freitas,
26 S., Andreae, M. O., and Artaxo, P.: Ground-based aerosol characterization during the South
27 American Biomass Burning Analysis (SAMBBA) field experiment, Atmos. Chem.
28 Phys., 14, 12069–12083, doi:10.5194/acp-14-12069-2014, 2014.



- 1 Brooke, J. K.: Airborne Observations of the Physical and Optical Properties of Atmospheric
2 Aerosol, PhD Thesis, School of Earth and Environment, University of Leeds, UK, 2014. Met
3 Office CASE project.
- 4 Capes, G., Johnson, B., McFiggans, G., Williams, P. I., Haywood, J., and Coe, H.: Aging of
5 biomass burning aerosols over West Africa: Aircraft measurements of chemical composition,
6 microphysical properties, and emission ratios, *J. Geophys. Res. Atmos.*, 113, D00C15,
7 doi:10.1029/2008JD009845, 2008.
- 8 Cusack, S., Slingo, A., Edwards, J., and Wild, M.: The radiative impact of a simple aerosol
9 climatology on the Hadley Centre climate model, *Q. J. Roy. Meteorol. Soc.*, 124, 2517–2526,
10 1998.
- 11 Darbyshire, E., and Johnson B.: The South American Biomass Burning Analysis (SAMBBA)
12 Field Experiment, Sept-Oct 2012, Brazil, Summary booklet. Available on request from the
13 authors, 2012.
- 14 Darbyshire, E., Morgan, W. T., Allan, J., Liu, D., Flynn, M., Dorsey, J., O’Shea, S., Johnson,
15 B., Szpek, K., Marengo, F., Haywood, J., Brito, J., Artaxo, P., Longo, K., Coe, H.: The
16 vertical distribution of biomass burning pollution over tropical South America – Perspectives
17 from airborne in-situ observations during SAMBBA, *In preparation*, 2016a.
- 18 Darbyshire, E., Morgan, W. T., Allan, J., Liu, D., Flynn, M., Dorsey, J., O’Shea, S.,
19 Trembath, J., Johnson, B., Szpek, K., Marengo, F., Haywood, J., Brito, J., Artaxo, P., Longo,
20 K., Coe, H.: Effect of fire regime on the physical and chemical properties of biomass burning
21 aerosol over tropical South America – Perspectives from airborne in-situ observations during
22 SAMBBA, *In preparation*, 2016b.
- 23 Darmenov, A. and da Silva, A.: The Quick Fire Emissions Dataset (QFED) –
24 Documentation of versions 2.1, 2.2 and 2.4 NASA Technical Report Series on
25 Global Modeling and Data Assimilation NASA TM-2013-104606 version 32
26 <http://gmao.gsfc.nasa.gov/pubs/docs/Darmenov609.pdf>, 2013
- 27 Dentener, F., Kinne, S., Bond, T., Boucher, O., Cofala, J., Generoso, S., Ginoux, P., Gong, S.,
28 Hoelzemann, J. J., Ito, A., Marelli, L., Penner, J., Putaud, J.-P., Textor, C., Schulz, M., Van
29 der Werf, G. R., and Wilson, J.: Emissions of primary aerosol and precursor gases in the
30 years 2000 and 1750 prescribed data-sets for AeroCom, *Atmos. Chem. Phys. Discuss.*, 6,
31 2703–2763, 2006, <http://www.atmos-chem-phys-discuss.net/6/2703/2006/>



- 1 Diehl, T., Heil, A., Chin, M., Pan, X., Streets, D., Schultz, M., and Kinne, S., 2012,
2 Anthropogenic, biomass burning, and volcanic emissions of black carbon, organic carbon,
3 and SO₂ from 1980 to 2010 for hindcast model experiments. , doi:10.5194/acpd-12-24895-
4 2012 , Atmospheric Chemistry and Physics Discussion 12 : 24895-24954
- 5 Derwent, R.G., Collins, W.J., Jenkin, M.E., and Johnson, C.E., The global distribution of
6 secondary particulate matter in a 3-D Lagrangian chemistry transport model, *J. Atmos.*
7 *Chem.*, 44, 57-95, 2003.
- 8 Dubovik, O. and King, M. D.: A flexible inversion algorithm for retrieval of aerosol
9 optical properties from Sun and sky radiance measurements, *J. Geophys. Res.*, 105,
10 20673–20696, 2000.
- 11 Dubovik, O., Sinyuk, A., Lapyonok, T., Holben, B. N., Mishchenko, M.,
12 Yang, P., et al.: Application of spheroid models to account for aerosol particle
13 nonsphericity in remote sensing of desert dust, *J. Geophys. Res.-Atmos.*, 111(D11),
14 D11208, doi:10.1029/2005JD006619, 2006.
- 15 Feingold, G., Remer, L. A., Ramaprasad, J., and Kaufman, Y. J.: Analysis of smoke impact
16 on clouds in Brazilian biomass burning regions: An extension of Twomey's approach, *J.*
17 *Geophys. Res.*, 106, 22907–22922, 2001.
- 18 Freitas, S. R., Longo, K. M., Chatfield, R., Latham, D., Silva Dias, M. A. F., Andreae, M. O.,
19 Prins, E., Santos, J. C., Gielow, R., and Carvalho Jr., J. A.: Including the sub-grid scale plume
20 rise of vegetation fires in low resolution atmospheric transport models, *Atmos. Chem. Phys.*,
21 7, 3385–3398, doi:10.5194/acp-7-3385-2007, 2007.
- 22 Gao, R.S., Schwarz, J. P., Kelly, K. K., Fahey, D. W., Watts, L. A., Thompson, T.L.,
23 Spackman, R, Slowik, J.G., Cross, E.S., Han, J.-H., Davidovits, P., Onasch, T.B., and
24 Worsnop, D.R., A Novel Method for Estimating Light-Scattering Properties of Soot Aerosols
25 Using a Modified Single-Particle Soot Photometer, *Aerosol Science and Technology*, 41:2,
26 125-135 (2007).
- 27 Giglio, L., Randerson, J. T., and van der Werf, G. R.: Analysis of daily, monthly, and
28 annual burned area using the fourth-generation global fire emissions database (GFED4) *J.*
29 *Geophys. Res. Biogeosci.*, 118, 317–328, doi:10.1002/jgrg.20042, 2013.
- 30 Guenther, A., Hewitt, C. N., Erickson, D., Fall, R., Geron, C., Graedel, T., Harley, P.,
31 Klinger, L., Lerdau, M., McKay, W. A., Pierce, T., Scholes, B., Steinbrecher, R., Tallamraju,



- 1 R., Taylor, J., and Zimmerman, P.: A global model of natural volatile organic compound
2 emissions, *J. Geophys. Res.*, 100, 8873–8892, 1995.
- 3 Granier, C., Bessagnet, B., Bond, T., D'Angiola, A., van der Gon, H. D., Frost, G. J., Heil, A.,
4 Kaiser, J. W., Kinne, S., Klimont, Z., Kloster, S., Lamarque, J. F., Liousse, C., Masui, T.,
5 Meleux, F., Mieville, A., Ohara, T., Raut, J. C., Riahi, K., Schultz, M. G., Smith, S. J.,
6 Thompson, A., van Aardenne, J., van der Werf, G. R., and van Vuuren, D. P.: Evolution of
7 anthropogenic and biomass burning emissions of air pollutants at global and regional
8 scales during the 1980-2010 period, *Clim. Change*, 109, 163–190, doi:10.1007/s10584-011-
9 0154-1, 2011.
- 10 Haywood, J. and Boucher, O.: Estimates of the direct and indirect radiative forcing due to
11 tropospheric aerosols: A review, *Rev. Geophys.*, 38, 513–543, 2000.
- 12 Haywood, J. M., Osborne, S. R., Francis, P. N., Keil, A., Formenti, P., Andreae, M. O., and
13 Kaye, P. H.: The mean physical and optical properties of regional haze dominated by
14 biomass burning aerosol measured from the C-130 aircraft during SAFARI 2000, *J. Geophys.*
15 *Res.-Atmos.*, 108(D13), 8473, doi:10.1029/2002JD002226, 2003.
- 16 Haywood, J. M., et al.: Overview of the Dust and Biomass-burning Experiment and African
17 Monsoon Multidisciplinary Analysis Special Observing Period-0, *J. Geophys. Res.*, 113,
18 D00C17, doi:10.1029/2008JD010077, 2008.
- 19 Hewitt, H. T., Copsey, D., Culverwell, I. D., Harris, C. M., Hill, R. S. R., Keen, A. B.,
20 McLaren, A. J., and Hunke E. C.: Design and implementation of the infrastructure of
21 HadGEM3: The next-generation Met Office climate modelling system. *Geosci. Model*
22 *Dev.*, 4, 223–253, 2011.
- 23 Hsu, N. C., Tsay, S.-C., King, M. D., and Herman, J. R.: Aerosol properties over bright-
24 reflecting source regions, *IEEE Trans. Geosci. Remote Sens.*, 42 (3), 557–569,
25 doi:10.1109/TGRS.2004.824067, 2004.
- 26 Hsu, N. C., Tsay, S.-C., King, M. D., and Herman, J. R.: Deep Blue retrievals of Asian
27 aerosol properties during ACE-Asia, *IEEE Trans. Geosci. Remote Sens.*, 44 (11), 3180–
28 3195, doi:10.1109/TGRS.2006.879540, 2006.
- 29 Ichoku, C. and Ellison, L.: Global top-down smoke-aerosol emissions estimation using
30 satellite fire radiative power measurements, *Atmos. Chem. Phys.*, 14, 6643–6667,
31 doi:10.5194/acp-14-6643-2014, 2014.



- 1 Johnson, B. T., Osborne, S. R., Haywood, J. M., and Harrison, M. A. J.: Aircraft
2 measurements of biomass burning aerosol over West Africa during DABEX, *J. Geophys.*
3 *Res.-Atmos.*, 113, D00C06, doi:10.1029/2007JD009451, 2008.
- 4 Johnson, B., T., Heese, B., McFarlane, S., Chazette, P., Jones, A. and Bellouin, N.:
5 Vertical distribution and radiative forcing of mineral dust and biomass-burning aerosols
6 over West Africa during DABEX, *J. Geophys. Res.*, 113, D00C12,
7 doi:10.1029/2008JD009848, 2008b.
- 8 Johnston, F. H., Henderson, B., Chen, Y., Randerson, J. T., Marlier, M., DeFries, R. S.,
9 Kinney, P., Bowman, D. M. J. S., and Brauer, M.: Estimated Global Mortality
10 Attributable to Smoke from Landscape Fires, *Environ. Health Perspect.*, 120, 695–701,
11 doi:10.1289/ehp.1104422, 2012.
- 12 Jolleys, M. D., Coe, H., McFiggans, G., Capes, G., Allan, J. D., Crosier, J.,
13 Williams, P. I., Allen, G., Bower, K. N., Jimenez, J. L., Russell, L. M., Grutter, M., and
14 Baumgardner, D.: Characterizing the Aging of Biomass Burning Organic Aerosol by Use
15 of Mixing Ratios: A Meta-analysis of Four Regions, *Environ. Sci. Tech.*, 46, 13093–
16 13102, doi:10.1021/es302386v, 2012.
- 17 Jones, A., Haywood, J. M., and Boucher, O.: Aerosol forcing, climate response and
18 climate sensitivity in the Hadley Centre climate model, *J. Geophys. Res.*, 112, D20211,
19 doi:10.1029/2007JD008688, 2007.
- 20 Kahn, R. A., Chen, Y., Nelson, D. L., Leung, F.-Y., Li, Q., Diner, D. J., and Logan, J. A.:
21 Wildfire smoke injection heights: two perspectives from space, *Geophys. Res. Lett.*, 35,
22 18–21, doi:10.1029/2007GL032165, 2008.
- 23 Kaiser, J. W., Heil, A., Andreae, M. O., Benedetti, A., Chubarova, N., Jones, L.,
24 Morcrette, J.-J., Razinger, M., Schultz, M. G., Suttie, M., and van der Werf, G. R.:
25 Biomass burning emissions estimated with a global fire assimilation system based on
26 observed fire radiative power, *Biogeosciences*, 9, 527–554, doi:10.5194/bg-9-527-2012,
27 2012.
- 28 Kaufman, Y. J., Hobbs, P. V., Kirchoff, V., et al.: Smoke, Clouds, and Radiation-Brazil
29 (SCAR-B) Experiment, *J. Geophys. Res.*, 103(D24), 31 783–31 808, 1998.
- 30 Kettle, A., Andreae, M., Amouroux, D., Andreae, T., Bates, T., Berresheim, H.,
31 Bingemer, H., Boniforti, R., Curran, M., DiTullio, G., Helas, G., Jones, G., Keller, M.,



- 1 Kiene, R., Leck, C., Levasseur, M., Malin, G., Maspero, M., Matrai, P., McTaggart, A.,
2 Mihalopoulos, N., Nguyen, B., Novo, A., Putaud, J., Rapsomanikis, S., Roberts, G.,
3 Schebeske, G., Sharma, S., Sim, R., Staubes, R., Turner, S., and Uher, G.: A global
4 database of sea surface dimethylsulfide (DMS) measurements and a procedure to predict
5 sea surface DMS as a function of latitude, longitude and month, *Global Biogeochemical*
6 *Cycles*, 13, 399–444, 1999.
- 7 Kolusu, S. R., Marsham, J. H., Mulcahy, J., Johnson, B., Dunning, C., Bush, M., and
8 Spracklen, D. V.: Impacts of Amazonia biomass burning aerosols assessed from short-
9 range weather forecasts, *Atmos. Chem. Phys.*, 15, 12251–12266, doi:10.5194/acp-15-
10 12251-2015, 2015.
- 11 Koren, I., Martins, J.V., Remer, L. A., Afargan, H.: Smoke invigoration versus inhibition
12 of clouds over the amazon. *Science*. 2008, 321:946–9, doi:10.5194/acp-14-9641-2014,
13 2008.
- 14 Kotchenruther, R. A., and P. V. Hobbs, Humidification factors of aerosols from biomass
15 burning in Brazil, *J. Geophys. Res.*, 103(D24), 32081–32089 (1998).
- 16 Kulmala, M., Petäjä, T., Mönkkönen, P., Koponen, I. K., Dal Maso, M., Aalto, P. P.,
17 Lehtinen, K. E. J., and Kerminen, V.-M.: On the growth of nucleation mode particles: source
18 rates of condensable vapor in polluted and clean environments, *Atmos. Chem. Phys.*, 5, 409-
19 416, doi:10.5194/acp-5-409-2005, 2005.
- 20 Lack, D. A., Cappa, C. D., Covert, D. S., Baynard, T., Massoli, P., Sierau, B., Bates, T. S.,
21 Quinn, P., Lovejoy, E. R., and Ravishankara, A. R.: Bias in filter-based aerosol light
22 absorption measurements due to organic aerosol loading: Evidence from ambient
23 measurements, *Aerosol Sci. Technol.*, 42(12), 1033–1041, 2008.
- 24 Lamarque, J.-F., Bond, T. C., Eyring, V., Granier, C., Heil, A., Klimont, Z., Lee, D.,
25 Liousse, C., Mieville, A., Owen, B., Schultz, M. G., Shindell, D., Smith, S. J., Stehfest,
26 E., Van Aardenne, J., Cooper, O. R., Kainuma, M., Mahowald, N., McConnell, J. R.,
27 Naik, V., Riahi, K., and van Vuuren, D. P.: Historical (1850–2000) gridded
28 anthropogenic and biomass burning emissions of reactive gases and aerosols:
29 methodology and application, *Atmos. Chem. Phys.*, 10, 7017–7039, doi:10.5194/acp-10-
30 7017-2010, 2010.



- 1 Levy, R. C., Remer, L. A., Mattoo, S., Vermote, E. F., and Kaufman, Y. J.: Second-
2 generation operational algorithm: Retrieval of aerosol properties over land from
3 inversion of Moderate Resolution Imaging Spectroradiometer spectral reflectance, *J.*
4 *Geophys. Res.*, 112, D13211, doi:10.1029/2006JD007811, 2007.
- 5 Levy, R. C., Remer, L. A., Kleidman, R. G., Mattoo, S., Ichoku, C., Kahn, R., and Eck,
6 T. F.: Global evaluation of the Collection 5 MODIS dark-target aerosol products over
7 land, *Atmos. Chem. Phys.*, 10, 103,999–10,420, doi:10.5194/acp-10-10399-2010, 2010.
- 8 Levy, R. C., Mattoo, S., Munchak, L. A., Remer, L. A., Sayer, A. M., and Hsu, N. C.:
9 The Collection 6 MODIS aerosol products over land and ocean, *Atmos. Meas. Tech.*
10 *Discuss.*, 6, 159–259, doi:10.5194/amtd-6-159-2013, 2013.
- 11 Liousse, C., Guillaume, B., Grégoire, J. M., Mallet, M., Galy, C., Pont, V., Akpo, A.,
12 Bedou, M., Castéra, P., Dungall, L., Gardrat, E., Granier, C., Konaré, A., Malavelle, F.,
13 Mariscal, A., Mieville, A., Rosset, R., Serça, D., Solmon, F., Tummon, F., Assamoi, E.,
14 Yoboué, V., and Van Velthoven, P.: Updated African biomass burning emission
15 inventories in the framework of the AMMA-IDAF program, with an evaluation of
16 combustion aerosols, *Atmos. Chem. Phys.*, 10, 9631-9646, doi:10.5194/acp-10-9631-
17 2010, 2010.
- 18 Liss, P. and Merlivat, L.: *The Role of Air-Sea Exchange in Geochemical Cycling*, chap.
19 *Air-sea gas exchange rates: Introduction and synthesis*, 113–127, D. Reidel, Norwell,
20 Mass., 1986.
- 21 Magi, B. I. and Hobbs, P. V.: Effects of humidity on aerosols in southern Africa during
22 the biomass burning season, *J. Geophys. Res.*, 108, 8495, doi:10.1029/2002JD002144,
23 2003.
- 24 Malavelle, F., Pont V., Mallet M., Solmon F., Johnson B., Leon J.-F., and Liousse C.:
25 Simulation of aerosol radiative effects over West Africa during DABEX and AMMA SOP-0,
26 *J. Geophys. Res.*, 116, D08205, doi:10.1029/2010JD014829, 2011.
- 27 Mann, G. W., Carslaw, K. S., Spracklen, D. V., Ridley, D. A., Manktelow, P. T.,
28 Chipperfield, M. P., Pickering, S. J., and Johnson, C. E.: Description and evaluation of
29 GLOMAP-mode: A modal global aerosol microphysics model for the UKCA
30 composition-climate model, *Geosci. Model Dev.*, 3, 519–551, doi:10.5194/gmd-3-519-
31 2010, 2010.



- 1 Mann, G. W., Carslaw, K. S., Reddington, C. L., Pringle, K. J., Schulz, M., Asmi, A.,
2 Spracklen, D. V., Ridley, D. A., Woodhouse, M. T., Lee, L. A., Zhang, K., Ghan, S. J.,
3 Easter, R. C., Liu, X., Stier, P., Lee, Y. H., Adams, P. J., Tost, H., Lelieveld, J., Bauer, S. E.,
4 Tsigaridis, K., van Noije, T. P. C., Strunk, A., Vignati, E., Bellouin, N., Dalvi, M., Johnson,
5 C. E., Bergman, T., Kokkola, H., von Salzen, K., Yu, F., Luo, G., Petzold, A., Heintzenberg,
6 J., Clarke, A., Ogren, J. A., Gras, J., Baltensperger, U., Kaminski, U., Jennings, S. G.,
7 O'Dowd, C. D., Harrison, R. M., Beddows, D. C. S., Kulmala, M., Viisanen, Y., Ulevicius,
8 V., Mihalopoulos, N., Zdimal, V., Fiebig, M., Hansson, H.-C., Swietlicki, E., and Henzing, J.
9 S.: Intercomparison and evaluation of global aerosol microphysical properties among
10 AeroCom models of a range of complexity, *Atmos. Chem. Phys.*, 14, 4679-4713,
11 doi:10.5194/acp-14-4679-2014, 2014.
- 12 Mao, J., Horowitz, L. W., Naik, V., Fan, S., Liu, J., and Fiore, A., M.: Sensitivity of
13 tropospheric oxidants to biomass burning emissions: implications for radiative forcing,
14 *Geophys. Res. Lett.*, 40, 1241–1246, doi:10.1002/grl.50210, 2013.
- 15 Marengo, F., Johnson, B., Langridge, J. M., Mulcahy, J., Benedetti, A., Remy, S., Jones,
16 L., Szpek, K., Haywood, J., Longo, K., and Artaxo, P.: On the vertical distribution of
17 smoke in the Amazonian atmosphere during the dry season, *Atmos. Chem. Phys.*, 16,
18 2155-2174, doi:10.5194/acp-16-2155-2016, 2016.
- 19 Marlier, M. E., DeFries, S. R., Voulgarakis, A., Kinney, P. L., Randerson, J. T., Shindell,
20 D. T., Chen, Y., and Faluvegi, G.: El Nino and health risks from landscape fire emissions
21 in southeast Asia, *Nature Climate Change*, 3, 131–136, doi:10.1038/nclimate1658,
22 2013.
- 23 Martin, S. T., Andreae, M. O., Artaxo, P., Baumgardner, D., Chen, Q., Goldstein, A. H.,
24 Guenther, A., Heald, C. L., Mayol Bracero, O. L., McMurry, P. H., Pauliquevis, T., Poschl,
25 U., Prather, K. A., Roberts, G. C., Saleska, S. R., Silva-Dias, M. A., Spracklen, D. V.,
26 Swietlicki, E., and Trebs, I.: Sources and properties of Amazonian aerosol particles, *Rev.*
27 *Geophys.*, 48, RG2002, doi:10.1029/2008RG000280, 2010.
- 28 Mercado, L., Bellouin, N., Stich, S., Boucher, O., Huntingford, C., Wild, M., and Wild,
29 P.: Impacts of changes in diffuse radiation on the global land carbon sink, *Nature*, 458,
30 01014–01018, doi:10.1028/nature07949, 2009.



- 1 Morgan, W., Allan, J., Flynn, M., Darbyshire, E., Liu, D., Szpek, K., Langridge J., Johnson,
2 B., Haywood, J., Longo, K. M., Artaxo, P., Coe, H.: Transformation of aerosol chemical
3 composition and resultant impact on climate during the South American Biomass Burning
4 Analysis (SAMBBA), iCACGP/IGAC-2014 Science Conference on Atmospheric Chemistry,
5 Brazil Natal, 22-26 September, 2014.
- 6 Morgenstern, O., Braesicke, P., O'Connor, F. M., Bushell, A. C., Johnson, C. E., Osprey,
7 S. M., and Pyle, J. A.: Evaluation of the new UKCA climate-composition model – Part 1:
8 The stratosphere, *Geosci. Model Dev.*, 2, 43-57, doi:10.5194/gmd-2-43-2009, 2009.
- 9 Milton, S. F., Greed G., Brooks, M. E., Haywood, J., Johnson, B., Allan, R. P., Slingo, A.,
10 and Grey, W. M. F.: Modeled and observed atmospheric radiation balance during the West
11 African dry season: Role of mineral dust, biomass burning aerosol, and surface albedo, *J.*
12 *Geophys. Res.*, 113, D00C02, doi:10.1029/2007JD009741, 2008.
- 13 Moteki, N., and Kondo Y.: Method to measure time-dependent scattering cross-sections of
14 particles evaporating in a laser beam, *J. Aerosol Sci.*, 39, doi:10.1016/j.jaerosci.2007.12.002,
15 2008.
- 16 Myhre, G., Samset, B. H., Schulz, M., Balkanski, Y., Bauer, S., Bernsten, T. K., Bian,
17 H., Bellouin, N., Chin, M., Diehl, T., Easter, R. C., Feichter, J., Ghan, S. J.,
18 Hauglustaine, D., Iversen, T., Kinne, S., Kirkevåg, A., Lamarque, J.-F., Lin, G., Liu, X.,
19 Lund, M. T., Luo, G., Ma, X., van Noije, T., Penner, J. E., Rasch, P. J., Ruiz, A., Seland,
20 Ø., Skeie, R. B., Stier, P., Takemura, T., Tsigaridis, K., Wang, P., Wang, Z., Xu, L., Yu,
21 H., Yu, F., Yoon, J.-H., Zhang, K., Zhang, H., and Zhou, C.: Radiative forcing of the
22 direct aerosol effect from AeroCom Phase II simulations, *Atmos. Chem. Phys.*, 13, 1853-
23 1877, doi:10.5194/acp-13-1853-2013, 2013.
- 24 Myhre, G., Hoyle C. R., Berglen T. F., Johnson B. T., and Haywood J. M.: Modeling of the
25 solar radiative impact of biomass burning aerosols during the Dust and Biomass-burning
26 Experiment (DABEX), *J. Geophys. Res.*, 113, D00C16, doi:10.1029/2008JD009857, 2008.
- 27 Ng, N. L., Canagaratna, M. R., Zhang, Q., Jimenez, J. L., Tian, J., Ulbrich, I.
28 M., Kroll, J. H., Docherty, K. S., Chhabra, P. S., Bahreini, R., Murphy, S. M.,
29 Seinfeld, J. H., Hildebrandt, L., Donahue, N. M., DeCarlo, P. F., Lanz, V. A., Prévôt,
30 A. S. H., Dinar, E., Rudich, Y., and Worsnop, D. R.: Organic aerosol components



- 1 observed in Northern Hemispheric datasets from Aerosol Mass Spectrometry,
2 Atmos. Chem. Phys., 10, 4625–4641, doi:10.5194/acp-10-4625-2010, 2010.
- 3 O'Connor, F. M., Johnson, C. E., Morgenstern, O., Abraham, N. L., Braesicke, P., Dalvi,
4 M., Folberth, G. A., Sanderson, M. G., Telford, P. J., Voulgarakis, A., Young, P. J.,
5 Zeng, G., Collins, W. J., and Pyle, J. A.: Evaluation of the new UKCA climate-
6 composition model – Part 2: The Troposphere, Geosci. Model Dev., 7, 41-91,
7 doi:10.5194/gmd-7-41-2014, 2014.
- 8 Ott, L., Duncan, B., Pawson, S., Colarco, P. R., Chin, M., Randles, C., Diehl, T., and
9 Nielsen, E.: The influence of the 2006 Indonesian biomass burning aerosols on tropical
10 dynamics studied with the GEOS-5 AGCM, J. Geophys. Res.,
11 doi:10.1029/2009JD013181, D14121, 2010.
- 12 Pacifico, F., Folberth, G. A., Sitch, S., Haywood, J. M., Rizzo, L. V., Malavelle, F. F., and
13 Artaxo, P.: Biomass burning related ozone damage on vegetation over the Amazon forest: a
14 model sensitivity study, Atmos. Chem. Phys., 15, 2791-2804, doi:10.5194/acp-15-2791-2015,
15 2015.
- 16 Petrenko, M., Kahn, R., Chin, M., Soja, A., Kucsera, T., and Harshvardhan, N.: The use of
17 satellite-measured aerosol optical depth to constrain biomass burning emissions source
18 strength in the global model GOCART, J. Geophys. Res., 117, D18212,
19 doi:10.1029/2012JD017870, 2012.
- 20 Ramanathan, V. and Carmichael, G.: Global and regional climate changes due to black
21 carbon, Nature Geosci., 1, 221–227, doi:10.1038/ngeo156, 2008.
- 22 Ramanathan, V., Crutzen, P. J., Kiehl, J. T., and Rosenfeld, D.: Aerosols, climate, and
23 the hydrological cycle, Science, 294, 2119–2124, 2001.
- 24 Rap, A., Spracklen, D. V., Mercado, L., Reddington, C. L., Haywood, J. M., Ellis, R. J.,
25 Phillips, O. L., Artaxo, P., Bonal, D., Coupe, N. R., and Butt, N.: Fires increase Amazon
26 forest productivity through increases in diffuse radiation, Geophys. Res. Lett., 42, 4654–
27 4662, doi:10.1002/2015GL063719, 2015.
- 28 Reddington, C. L., Butt, E. W., Ridley, D. A., Artaxo, P., Morgan, W. T., Coe, H., and
29 Spracklen, D. V.: Air quality and human health improvements from reductions in
30 deforestation-related fire in Brazil. Nature Geoscience 8, 768–771
31 doi:10.1038/ngeo2535, 2015.



- 1 Reddington, C. L., Spracklen, D. V., Artaxo, P., Ridley, D., Rizzo, L. V., and Arana, A.:
2 Analysis of particulate emissions from tropical biomass burning using a global aerosol model
3 and long-term surface observations, Atmos. Chem. Phys. Discuss., doi:10.5194/acp-2015-
4 967, in review, 2016.
- 5 Reid, J. S., Koppmann, R., Eck, T. F., and Eleuterio, D. P.: A review of biomass burning
6 emissions part II: intensive physical properties of biomass burning particles, Atmos.
7 Chem. Phys., 5, 799-825, doi:10.5194/acp-5-799-2005, 2005.
- 8 Reid, J. S., Eck, T. F., Christopher, S. A., Koppmann, R., Dubovik, O., Eleuterio, D. P.,
9 Holben, B. N., Reid, E. A., and Zhang, J.: A review of biomass burning emissions part III:
10 intensive optical properties of biomass burning particles, Atmos. Chem. Phys., 5, 827-849,
11 doi:10.5194/acp-5-827-2005, 2005b.
- 12 Remer, L., Kaufman, Y., Tanre, D., Mattoo, S., Chu, D., Martins, J., et al.: The MODIS
13 aerosol algorithm, products, and validation, J. Atmos. Sci., 62(4), 947–973, 2005.
- 14 Reynolds, R. W., Smith, T. M., Liu, C., Chelton, D. B., Casey, K. S., and Schlax,
15 M. G.: Daily High-Resolution-Blended Analyses for Sea Surface Temperature, J.
16 Climate, 20, 5473–5496, doi:10.1175/2007JCLI1824.1, 2007.
- 17 Saleh, R., Robinson, E. S., Tkacik, D. S., Ahern, A. T., Liu, S., Aiken, A. C., Sullivan, R. C.,
18 Presto, A. A., Dubey, M. K., Yokelson, R. J., Donahue, N. M., and Robinson, A. L.:
19 Brownness of organics in aerosols from biomass burning linked to their black carbon content,
20 Nat. Geosci., 7, 647–650, 2014.
- 21 Samset, B. H., Myhre, G., Schulz, M., Balkanski, Y., Bauer, S., Berntsen, T. K., Bian,
22 H., Bellouin, N., Diehl, T., Easter, R. C., Ghan, S. J., Iversen, T., Kinne, S., Kirkevåg,
23 A., Lamarque, J.-F., Lin, G., Liu, X., Penner, J. E., Seland, Ø., Skeie, R. B., Stier, P.,
24 Takemura, T., Tsigaridis, K., and Zhang, K.: Black carbon vertical profiles strongly
25 affect its radiative forcing uncertainty, Atmos. Chem. Phys., 13, 2423–2434,
26 doi:10.5194/acp-13-2423-
27 2013, 2013.
- 28 Sayer, A. M., Munchak, L. A., Hsu, N. C., Levy, R. C., Bettenhausen, C., and Jeong M.-
29 J.: MODIS Collection 6 aerosol products: Comparison between Aqua's e-Deep Blue,
30 Dark Target, and “merged” data sets, and usage recommendations, J. Geophys. Res.
31 Atmos., 119, 13,965–13,989, doi:10.1002/2014JD022453, 2014.



- 1 Shindell, D. T., Lamarque, J.-F., Schulz, M., Flanner, M., Jiao, C., Chin, M., Young, P. J.,
2 Lee, Y. H., Rotstaysn, L., Mahowald, N., Milly, G., Faluvegi, G., Balkanski, Y., Collins, W. J.,
3 Conley, A. J., Dalsoren, S., Easter, R., Ghan, S., Horowitz, L., Liu, X., Myhre, G.,
4 Nagashima, T., Naik, V., Rumbold, S. T., Skeie, R., Sudo, K., Szopa, S., Takemura, T.,
5 Voulgarakis, A., Yoon, J.-H., and Lo, F.: Radiative forcing in the ACCMIP historical and
6 future climate simulations, *Atmos. Chem. Phys.*, 13, 2939-2974, doi:10.5194/acp-13-2939-
7 2013, 2013.
- 8 Schutgens, N. A. J., Partridge, D. G., and Stier, P.: The importance of temporal
9 collocation for the evaluation of aerosol models with observations, *Atmos. Chem. Phys.*,
10 *Discuss.*, 15, 26191-26230, doi:10.5194/acpd-15-26191-2015, 2015.
- 11 Sofiev, M., Ermakova, T., and Vankevich, R.: Evaluation of the smoke-injection height
12 from wild-land fires using remote-sensing data, *Atmos. Chem. Phys.*, 12, 1995–2006,
13 doi:10.5194/acp-12-1995-2012, 2012.
- 14 Spracklen, D. V., Carslaw, K. S., Pöschl, U., Rap, A., and Forster, P. M.: Global cloud
15 condensation nuclei influenced by carbonaceous combustion aerosol, *Atmos. Chem.*
16 *Phys.*, 11, 9067-9087, doi:10.5194/acp-11-9067-2011, 2011.
- 17 Stier, P., Feichter, J., Kinne, S., Kloster, S., Vignati, E., Wilson, J., Ganzeveld, L.,
18 Tegen, I., Werner, M., Balkanski, Y., Schulz, M., Boucher, O., Minikin, A., and Petzold,
19 A.: The aerosol-climate model ECHAM5-HAM, *Atmos. Chem. Phys.*, 5, 1125–1156,
20 doi:10.5194/acp-5-1125-2005, 2005.
- 21 IPCC: Climate Change 2013: The Physical Science Basis: Sum-
22 mmary for Policymakers, Cambridge, UK, 2013.
- 23 Stokes, R. H., and Robinson, R. A.: Interactions in aqueous nonelectrolyte solutions, solute-
24 solvent equilibria, *J. Phys. Chem.*, 70(7), 2126–2131, 1966.
- 25 Swap, B., Annegarn H. J., Suttles, J. T., Haywood, J., Helmlinger M. C., Hely C., Hobbs, P.
26 V., Holben B., Ji, J., King, M. D., Landmann T., Maenhaut W., Otter L., Pak B., Piketh, S. J.,
27 Platnick, S., Privette, J. L., Roy, D., Thompson, A. M., Ward, D., and Yokelson, R.: The
28 Southern African Regional Science Initiative (SAFARI 2000): Overview of the dry season
29 field campaign, *S. African J. Sci.*, 98, 125-130, 2002.



- 1 Swietlicki, E., Hansson, H. C., Hameri, K., Svenningsson, B., Massling, A., McFiggans,
2 G., McMurry, P., Petaja, T., Tunved, P., Gysel, M., Topping, D., Weingartner, E.,
3 Baltensperger, U., Rissler, J., Wiedensohler, A., and Kulmala, M.: Hygroscopic
4 properties of submicrometer atmospheric aerosol particles measured with H TDMA
5 instruments in various environments – A review, *Tellus B*, 60, 432–469, 2008.
- 6 Ten Hoeve, J. E., Jacobson, M. Z., and Remer, L. A.: Comparing results from a physical
7 model with satellite and in situ observations to determine whether biomass burning aerosols
8 over the Amazon brighten or burn off clouds, *J. Geophys. Res.*, 117, D08203,
9 doi:10.1029/2011JD016856, 2012.
- 10 Tiitta, P., Vakkari, V., Josipovic, M., Croteau, P., Beukes, J. P., van Zyl, P. G., Venter,
11 A. D., Jaars, K., Pienaar, J. J., Ng, N. L., Canagaratna, M. R., Jayne, J. T.,
12 Kerminen, V.-M., Kulmala, M., Laaksonen, A., Worsnop, D. R., and Laakso, L.:
13 Chemical composition, main sources and temporal variability of PM₁ aerosols in
14 southern African grassland, *Atmos. Chem. Phys.*, 14, 1909–1927, doi:10.5194/acp-14-
15 1909-2014, 2014.
- 16 Tosca, M. G., Randerson, J. T., Zender, C. S., Flanner, M. G., and Rasch, P. J.: Do
17 biomass burning aerosols intensify drought in equatorial Asia during El Nino?, *Atmos.*
18 *Chem. Phys.*, 10, 3515–3528, doi:10.5194/acp-10-3515-2010, 2010
- 19 Tosca, M. G., Randerson, J. T., Zender, C. S., Nelson, D. L., Diner, D. J., and Logan, J.
20 A.: Dynamics of fire plumes and smoke clouds associated with peat and deforestation
21 fires in Indonesia, *J. Geophys. Res.*, 116, 1–14, doi:10.1029/2010JD015148, 2011.
- 22 Tosca, M. G., Randerson, J. T., and Zender, C. S.: Global impact of smoke aerosols from
23 landscape fires on climate and the Hadley circulation, *Atmos. Chem. Phys.*, 13, 5227–
24 5241, doi:10.5194/acp-13-5227-2013, 2013.
- 25 Tosca, M. G., Diner, D. J., Garay, M. J., and Kalashnikova, O. V.: Observational
26 evidence of fire-driven reduction of cloud fraction in tropical Africa, *J. Geophys. Res.*
27 *Atmos.*, 119, 8418–8432, doi:10.1002/2014JD021759, 2014.
- 28 Turpin, B. J., Saxena, P., and Andrews, E.: Measuring and simulating particulate
29 organics in the atmosphere: problems and prospects, *Atmos. Environ.*, 34, 2983–
30 3013, 2000.



- 1 Turpin, B. J., and Lim, H. J.: Species Contributions to PM_{2.5} Mass Concentrations:
2 Revisiting Common Assumptions for Estimating Organic Mass, *Aerosol Sci.* 35, 602–610,
3 2001.
- 4 Twomey, S.: Pollution and the planetary albedo, *Atmos. Environ.*, 8, 1251–1256, 1974.
- 5 Val Martin, M., Logan, J. A., Kahn, R. A., Leung, F.-Y., Nelson, D. L., and Diner, D. J.:
6 Smoke injection heights from fires in North America: analysis of 5 years of satellite
7 observations, *Atmos. Chem. Phys.*, 10, 1491–1510, doi:10.5194/acp-10-1491-2010, 2010.
- 8 Val Martin, M., Kahn, R. A., Logan, J. A., Paugam, R., Wooster, M., and Ichoku, C.:
9 Space-based observational constraints for 1-D fire smoke plume-rise models, *J. Geophys.*
10 *Res.*, 117, D22204, doi:10.1029/2012JD018370, 2012.
- 11 Vakkari, V., Kerminen, V.-M., Beukes, J., Tiitta, P., van Zyl, P., Josipovic, M., Venter,
12 A., Jaars, K., Worsnop, D., Kulmala, M., and Laakso, L.: Rapid changes in biomass
13 burning aerosols by atmospheric oxidation, *Geophys. Res. Lett.*, 41, 2644–2651,
14 doi:10.1002/2014GL059396, 2014.
- 15 van der Werf, G. R., Randerson, J. T., Giglio, L., Collatz, G. J., Mu, M., Kasibhatla, P. S.,
16 Morton, D. C., DeFries, R. S., Jin, Y., and van Leeuwen, T. T.: Global fire emissions and the
17 contribution of deforestation, savanna, forest, agricultural, and peat fires (1997–2009), *Atmos.*
18 *Chem. Phys.*, 10, 11707–11735, doi:10.5194/acp-10-11707-2010, 2010.
- 19 Voulgarakis, A., and Field, R. D.: Fire influences on atmospheric composition, air quality,
20 and climate. *Curr. Pollut. Rep.*, 1, no. 2, 70–81, doi:10.1007/s40726-015-0007-z, 2015.
- 21 Walters, D. N., Williams, K. D., Boutle, I. A., Bushell, A. C., Edwards, J. M., Field, P.
22 R., Lock, A. P., Morcrette, C. J., Stratton, R. A., Wilkinson, J. M., Willett, M. R.,
23 Bellouin, N., Bodas-Salcedo, A., Brooks, M. E., Copsey, D., Earnshaw, P. D., Hardiman,
24 S. C., Harris, C. M., Levine, R. C., MacLachlan, C., Manners, J. C., Martin, G. M.,
25 Milton, S. F., Palmer, M. D., Roberts, M. J., Rodríguez, J. M., Tennant, W. J., and
26 Vidale, P. L.: The Met Office Unified Model Global Atmosphere 4.0 and JULES Global
27 Land 4.0 configurations, *Geosci. Model Dev.*, 7, 361–386, doi:10.5194/gmd-7-361-2014,
28 2014.
- 29 Ward, D. S., Kloster, S., Mahowald, N. M., Rogers, B. M., Randerson, J. T., and Hess, P.
30 G.: The changing radiative forcing of fires: global model estimates for past, present and
31 future, *Atmos. Chem. Phys.*, 12, 10857–10886, doi:10.5194/acp-12-10857-2012, 2012.



- 1 World Climate Programme (WCP): Report of the experts meeting on aerosols and their
2 climatic effects, edited by Deepak, A. and Gerber, H. G., World Meteorological Organization,
3 Geneva, Switzerland, Rep. WCP-55, 107 pp., 1983.
- 4 Williams, K. D., Harris, C. M., Bodas-Salcedo, A., Camp, J., Comer, R. E., Copsey, D.,
5 Fereday, D., Graham, T., Hill, R., Hinton, T., Hyder, P., Ineson, S., Masato, G., Milton,
6 S. F., Roberts, M. J., Rowell, D. P., Sanchez, C., Shelly, A., Sinha, B., Walters, D. N.,
7 West, A., Woollings, T., and Xavier, P. K.: The Met Office Global Coupled model 2.0
8 (GC2) configuration, *Geosci. Model Dev.*, 8, 1509-1524, doi:10.5194/gmd-8-1509-2015,
9 2015.
- 10 Whitehead, J. D., Irwin, M., Allan, J. D., Good, N., and McFiggans, G.: A meta-analysis of
11 particle water uptake reconciliation studies, *Atmos. Chem. Phys.*, 14, 11833-11841,
12 doi:10.5194/acp-14-11833-2014, 2014.
- 13 Woodward, S.: Modelling the atmospheric life cycle and radiative impact of mineral dust in
14 the Hadley Centre climate model, *J. Geophys. Res.*, 106, 18155–18166, 2001.
- 15 Woodward, S.: Mineral Dust in HadGEM2, Hadley Centre Technical Note 87, Met Office
16 Hadley Centre for Climate Change, Exeter, United Kingdom,
17 <http://www.metoffice.gov.uk/archive/science/climatescience/hctn87>, 2011.
- 18 Wu, P., Christidis, N. and Stott, P.: Anthropogenic impact on Earth's hydrological cycle *Nat.*
19 *Clim. Change*, 3, 807–10, doi:10.1038/nclimate1932, 2013.
- 20 Xia, L., Robock, A., Tilmes, S., and Neely III, R. R.: Stratospheric sulfate
21 geoengineering enhances terrestrial gross primary productivity, *Atmos. Chem. Phys.*
22 *Discuss.*, 15, 25627-25645, doi:10.5194/acpd-15-25627-2015, 2015.
- 23 Zhang, Y., R. Fu, H. Yu, Y. Qian, R. Dickinson, M. A. F. Silva Dias, P. L. da Silva Dias,
24 and K. Fernandes (2009), Impact of biomass burning aerosol on the monsoon circulation
25 transition over Amazonia, *Geophys. Res. Lett.*, 36, L10814, doi:10.1029/2009GL037180.
26



Aerosol scheme	Emitted particle properties			Scaling factors applied		
	D _g	σ	BC:OC	POM:OC conversion	Ageing growth factor	Global emission scaling
CLASSIC	0.20	1.3	0.093	n/a	1.62	1.6
GLOMAP-mode	0.15	1.59	Variable (GFED3.1)	1.4	n/a	2.0

1

2 **Table 1.** Biomass burning aerosol emissions: emitted particle properties and scaling factors
 3 applied.



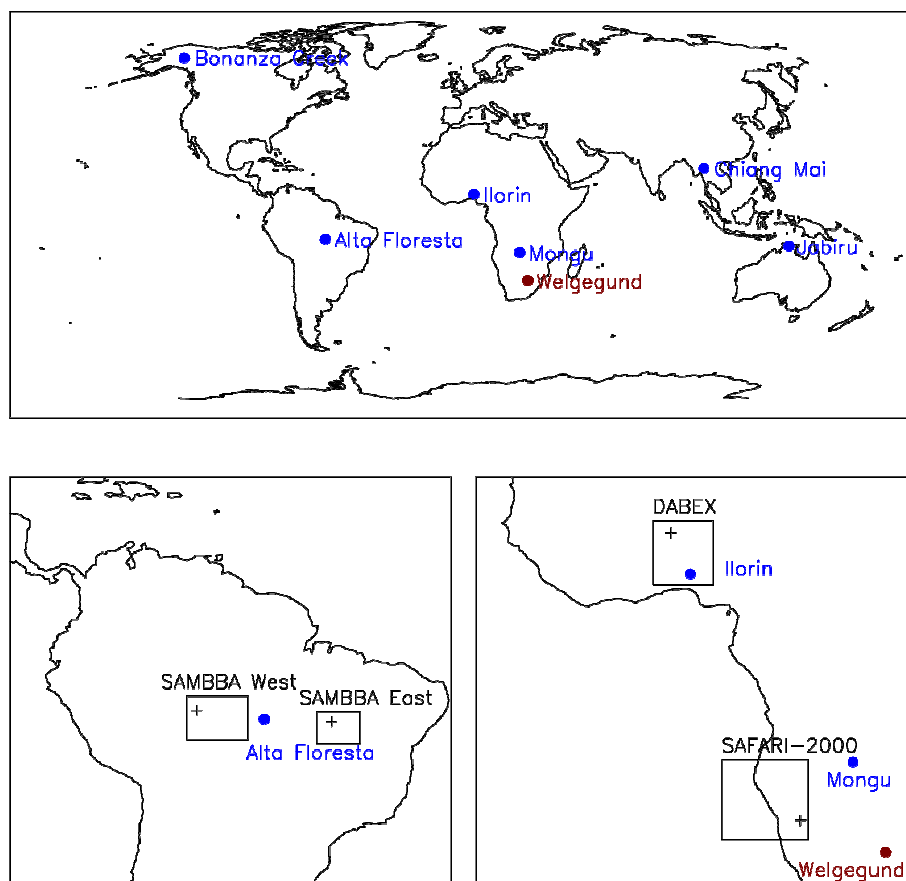
Data source	Campaign region	SSA	\AA	$k_{\text{ext,fm}}$ (m^2/g)	g	References
<i>models</i>						
CLASSIC	Global	0.91	2.3	5.0	0.58	Haywood et al. (2003)
aged BBA						
GLOMAP-mode fine-mode	SAMBBA West (Rondonia)	0.87	2.0	4.8	0.63	
	SAMBBA East (Tocantins)	0.86	2.1	4.5	0.60	
	DABEX (West Africa)	0.85	2.0	4.6	0.61	
	SAFARI (S. Africa)	0.86	2.0	4.8	0.62	
<i>Observations</i>						
In-situ aircraft observations	SAMBBA West (Phase 1, Rondonia) ^b	0.88 +/- 0.05	1.9 +/- 0.3	3.6 +/- 0.06	^c 0.66 +/- 0.05 ^d 0.59 +/- 0.05	Darbyshire et al. (in preparation, 2016b), Brooke (2014)
	SAMBBA East (Tocantins)	0.79	2.1 +/- 0.2	n/a	0.57 +/- 0.05	Darbyshire et al. (in preparation, 2016b).
	DABEX (West Africa)	0.81 +/- 0.05	1.7	5.8	0.63	Johnson et al. (2008)
	SAFARI-2000 (S. Africa)	0.88 +/- 0.04	n/a	4.3	0.58	Haywood et al. (2003) ^e

1

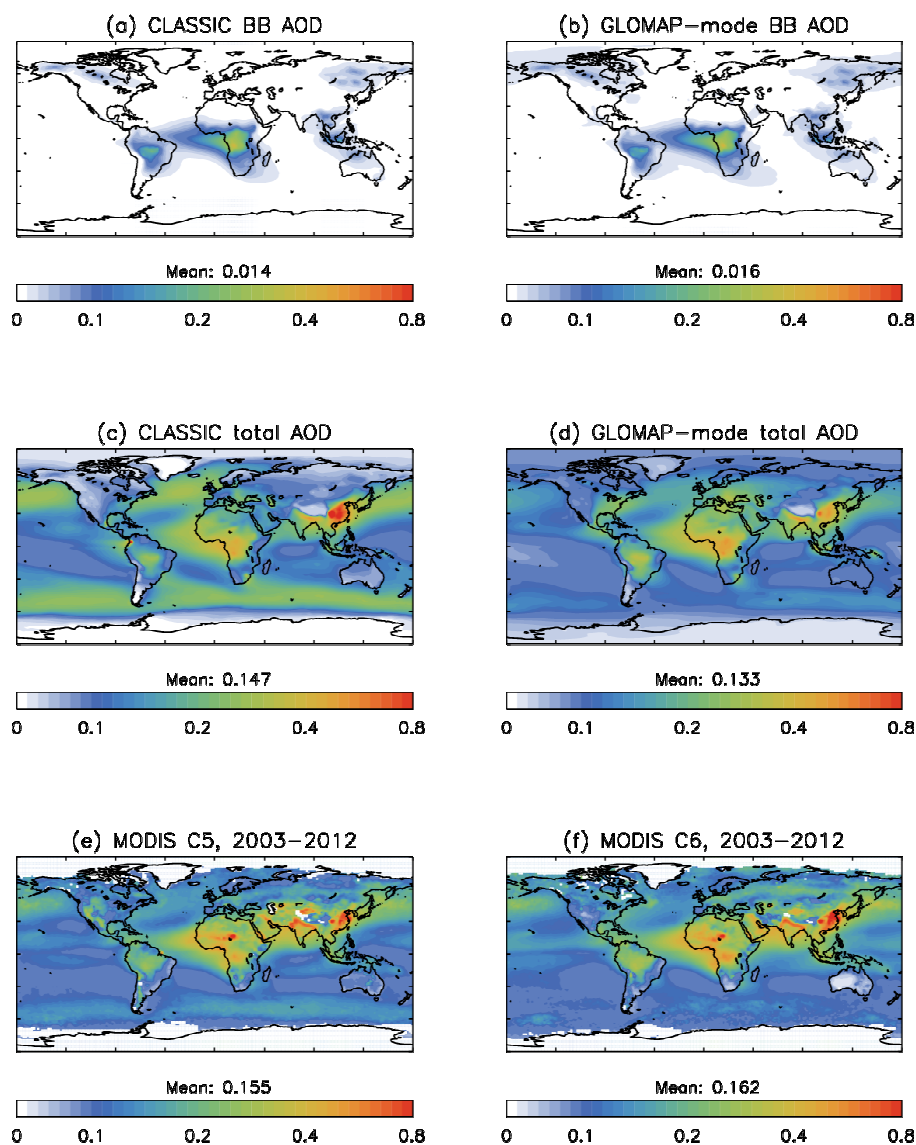
2 **Table 2.** Dry aerosol optical properties at 550nm from model and observations including Single Scattering
 3 Albedo (SSA), Ångström exponent (\AA), fine-mode specific extinction coefficient ($k_{\text{ext,fm}}$), and asymmetry
 4 parameter (g). Error bounds are given to observed parameters, where available, to reflect uncertainty in
 5 the measurement.



- 1 ^a Assuming a representative mixture with 10 % fresh and 90 % aged BB aerosol.
- 2 ^b Phase 1 of SAMBBA was from 14 – 22 September 2012.
- 3 ^c Calculated from the nephelometer backscatter fraction based on Andrew et al. (2006).
- 4 ^d Derived from Mie calculations in Brooke (2014)
- 5 ^e Haywood et al. (2003) results for SSA reassessed in Johnson et al. (2008).
- 6

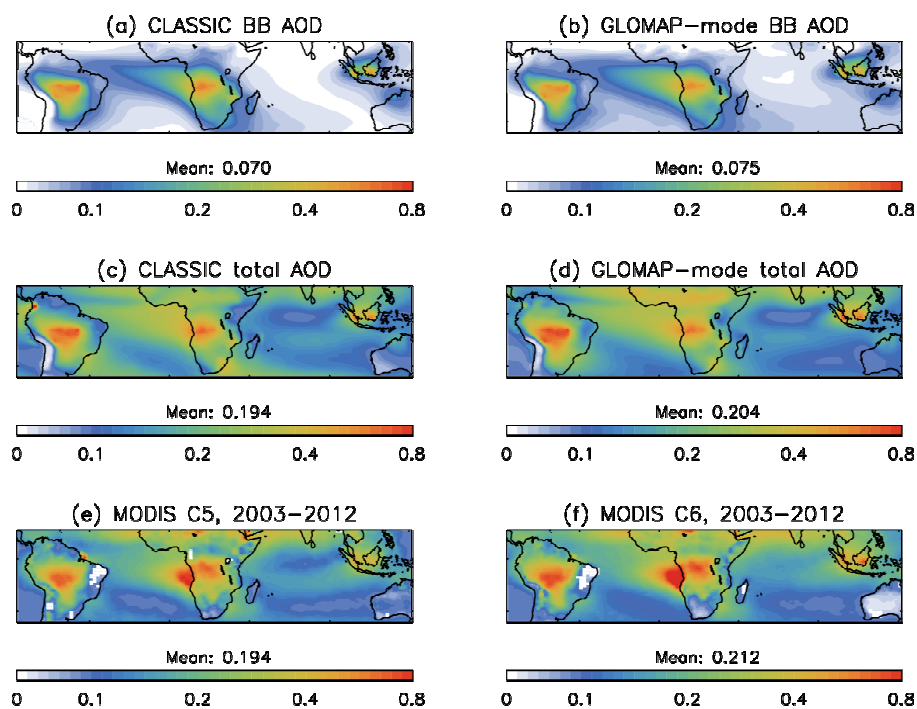


7
8 **Figure 1.** Maps showing the location of AERONET sites (blue), the Welgegund ground
9 station, and the averaging boxes used corresponding to the flight regions from SAMBBA
10 (West and East), DABEX and SAFARI-2000. Plus symbols indicate the locations of the main
11 airbases used for the flights: Porto Velho for SAMBBA West, Palmas for SAMBBA East,
12 Niamey for DABEX, and Windhoek for SAFARI-2000.



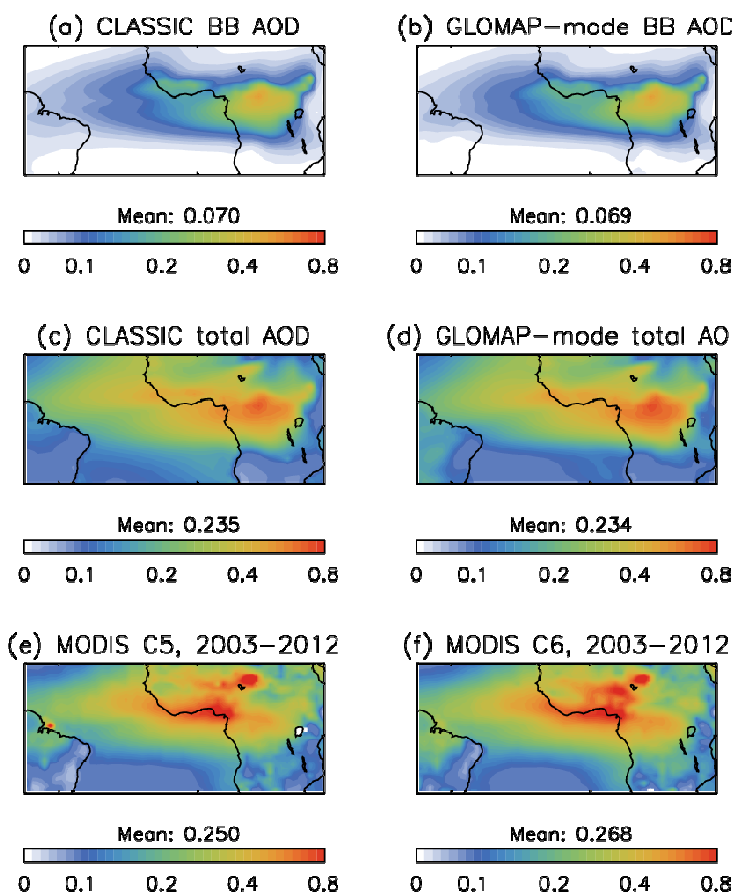
1

2 **Figure 2.** Decadal mean AOD at 550nm from the model simulations and MODIS. BB AOD
3 is the contribution of BBA emissions to the total AOD. Model means from 2002 – 2011 and
4 MODIS from 2003 – 2012 based on Aqua.



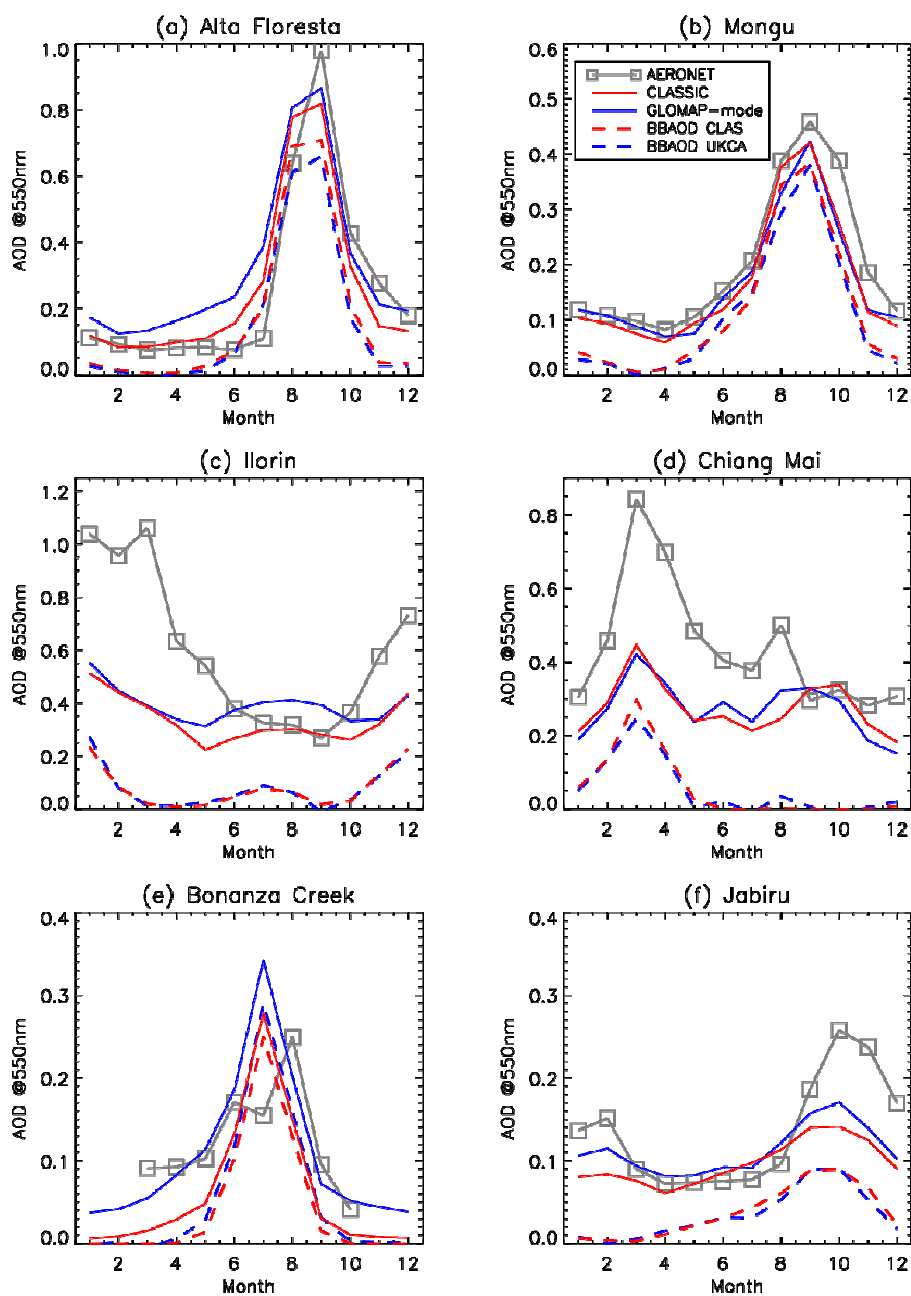
1

2 **Figure 3.** Same as Fig 2 but for the month of September.



1

2 **Figure 4.** Same as Fig 2 but for the month of January.

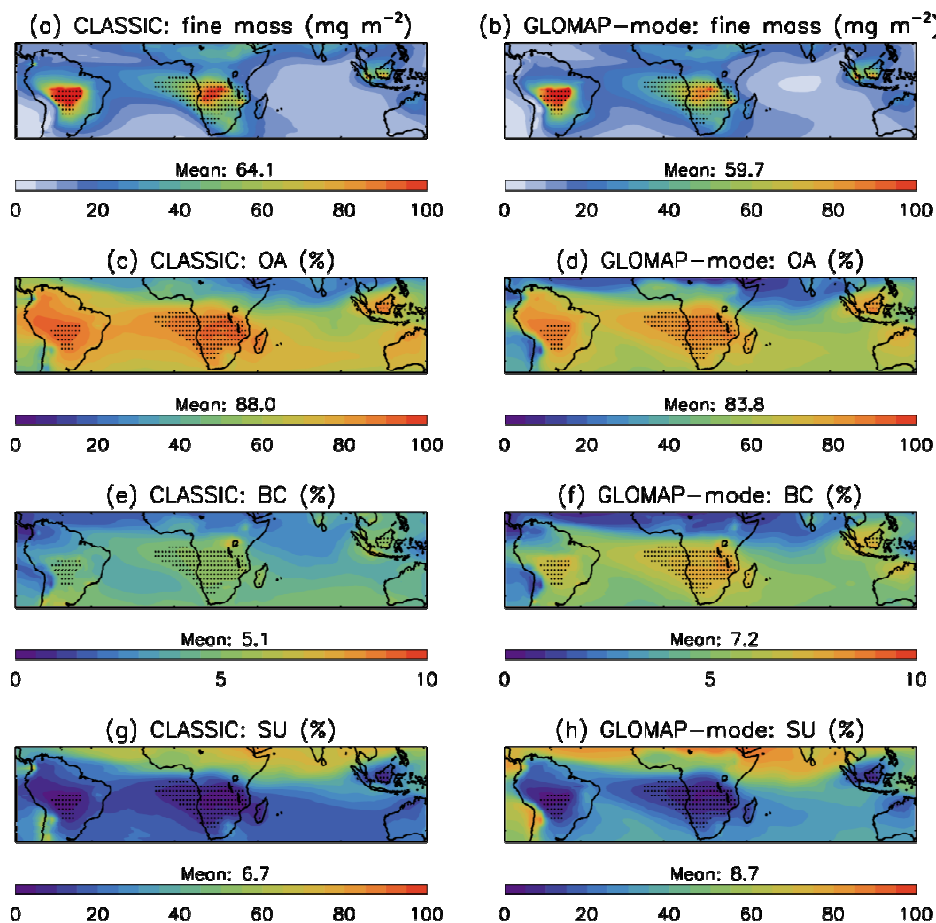


1

2 **Figure 5.** Monthly mean AOD at 550nm from six AERONET sites (grey squares), and the
3 same locations from GLOMAP-mode (blue) and CLASSIC (red). The contribution to AOD
4 from BBA is shown by dashed lines.



1

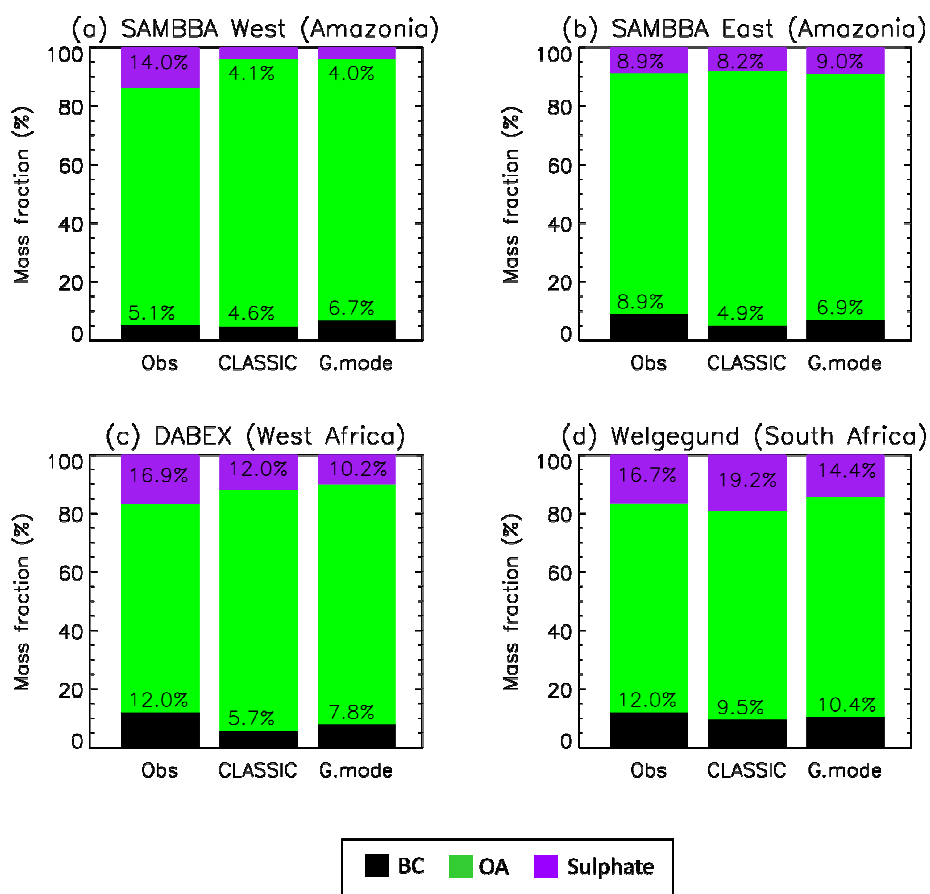


2

3

4 **Figure 6.** Modelled fine-mode aerosol composition from HadGEM3 for CLASSIC and
5 GLOMAP-mode (including sulphate, BC and OA only). Plots show: (a, b) fine-mode
6 mass burden (mg m^{-2}), (c, d) mass fraction of OA (%), (e, f) mass fraction of BC (%), (g,
7 h) mass fraction of sulphate (%). Stipples indicate grid columns where more than 75 % of
8 the fine-mode aerosol mass originates from biomass burning emissions (based on the
9 speciation in the CLASSIC simulation). Mean values beneath each plot give the average from
10 grid columns marked by these stipples.

11

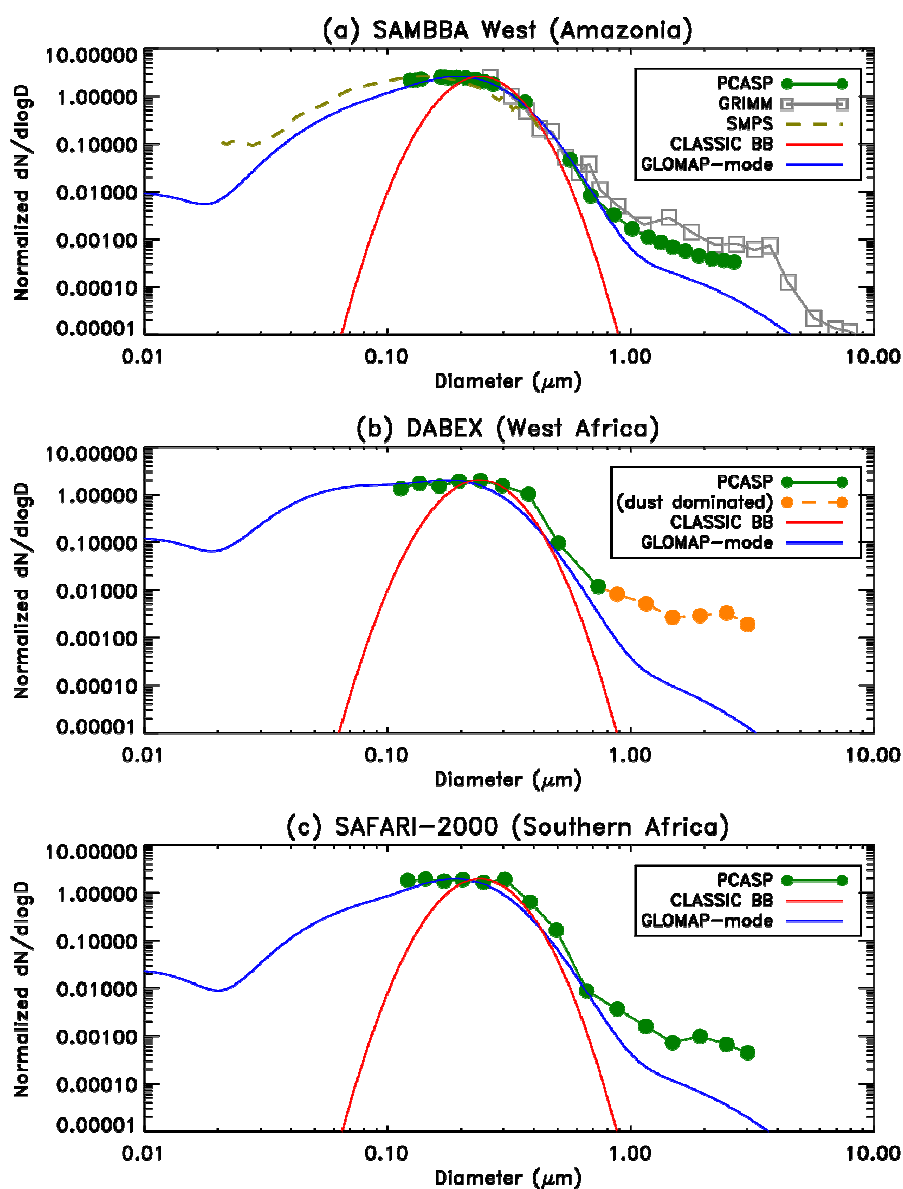


1

2

3

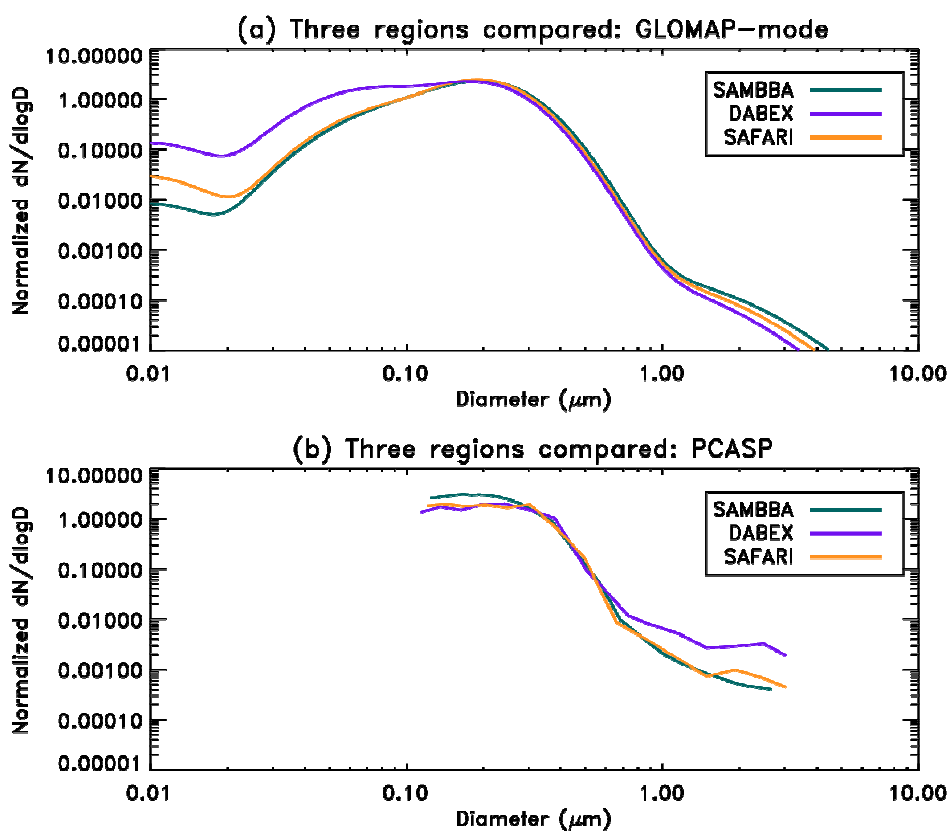
4 **Figure 7.** Mass fractions (%) of black carbon (black), organic aerosol (green), and
5 sulphate (purple) (excluding other fine-mode aerosol components). Observed data are
6 monthly averages from field campaigns including: SAMBBA (Amazonia, September
7 2012), DABEX (West Africa, Jan 2006), and the Welgegund site (South Africa,
8 September 2010). Modelled data are long-term monthly mean values corresponding to
9 the month and location of the observations. Welgegund model data is for aerosol
10 composition at the surface (lowest model level), SAMBBA and DABEX model data is
11 averaged over 0 – 5km. The BC and sulphate mass fractions are labelled on each bar.



1

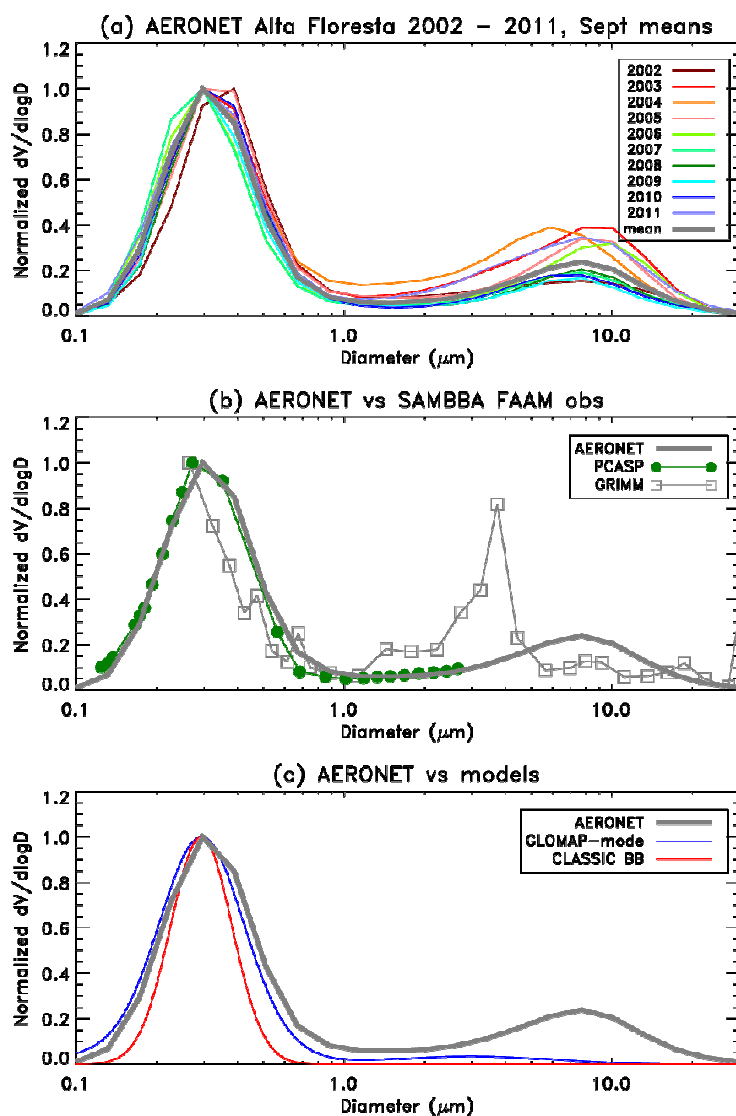
2 **Figure 8.** Aerosol number size distributions (dN/dlogD) versus particle diameter from aircraft
3 observations (PCASP, GRIMM, SMPS) showing the mean distribution from three campaigns.
4 CLASSIC curve is a representative mixture of 10 % fresh and 90 % aged BBA species,
5 GLOMAP-mode is the complete size distribution over all 5 modes averaged over the flight
6 regions in Fig. 1 and over 0 – 5km.

7



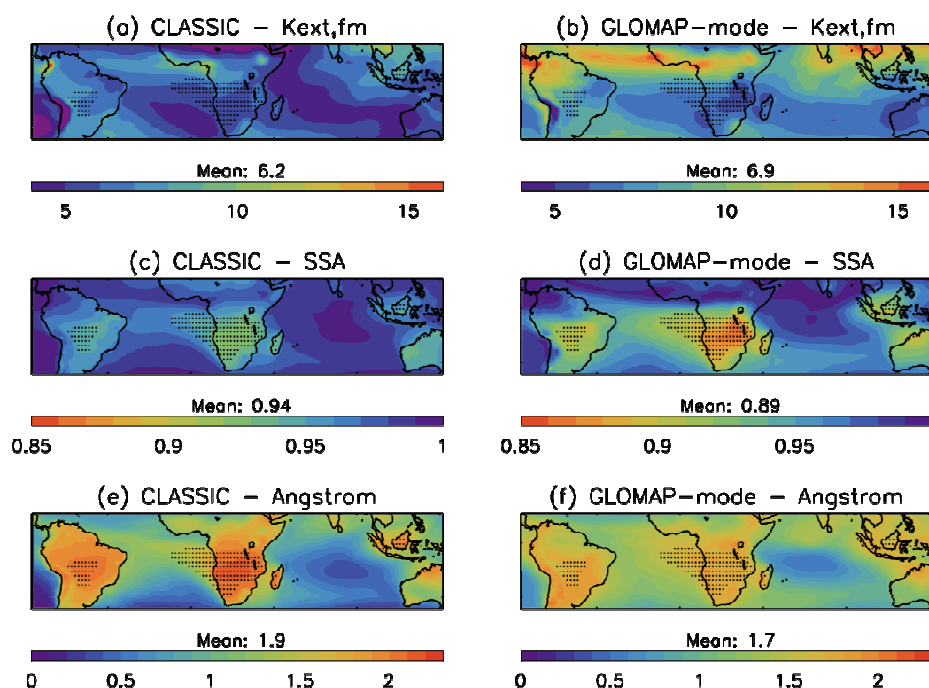
1

2 **Figure 9.** Same as Fig. 7 but showing only GLOMAP-mode curves and PCACP data.



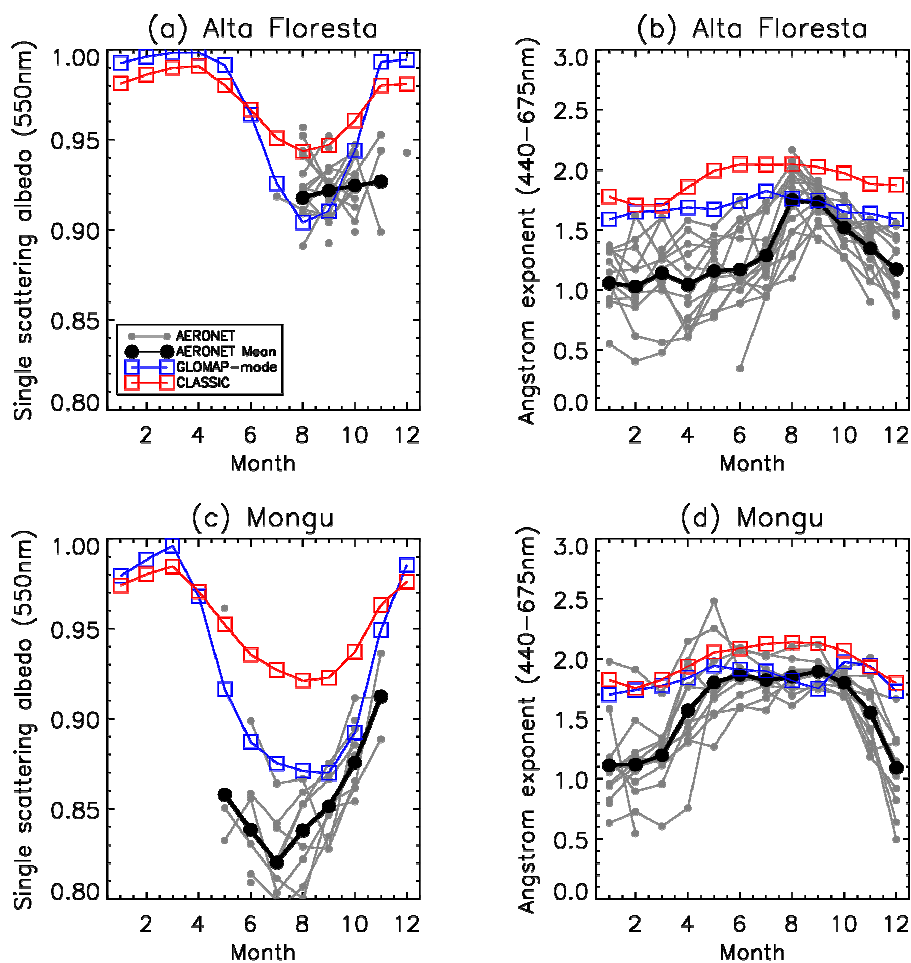
1

2 **Figure 10.** Aerosol volume size distributions ($dV/d\log D \mu\text{m}^3/\mu\text{m}^2$) vs. particle diameter for
3 (a) September means from AERONET Alta Floresta (Southern Amazonia) for 2002-2011
4 along with the long-term monthly mean from all years, (b) Comparison of AERONET 10-
5 year September mean with FAAM averages from SAMBBA West region, normalized by peak
6 concentration, (c) Comparison of AERONET 10-year September mean with HadGEM3
7 September monthly mean output, column-integrated mean over Alta Floresta for GLOMAP-
8 mode (all active size modes) and CLASSIC (BB species only).



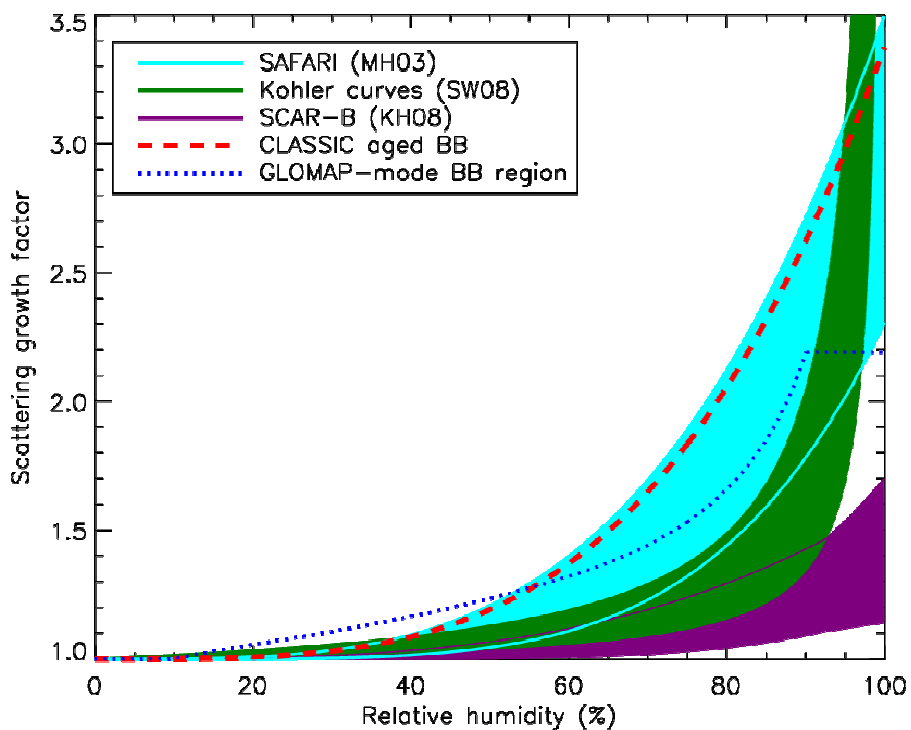
1
2

3 **Figure 11.** Column average moist aerosol optical properties from CLASSIC and GLOMAP-
4 mode for September long-term monthly mean. Properties are the fine-mode specific
5 extinction coefficient ($k_{ext, fm}$), Single Scattering Albedo (SSA) and Ångström exponent.
6 Stipples indicate grid columns where more than 75 % of the fine-mode aerosol mass
7 originates from biomass burning emissions (based on the speciation in the CLASSIC
8 simulation). Mean values beneath each plot give the average from grid columns marked by
9 these stipples.



1
2
3
4
5
6
7
8
9

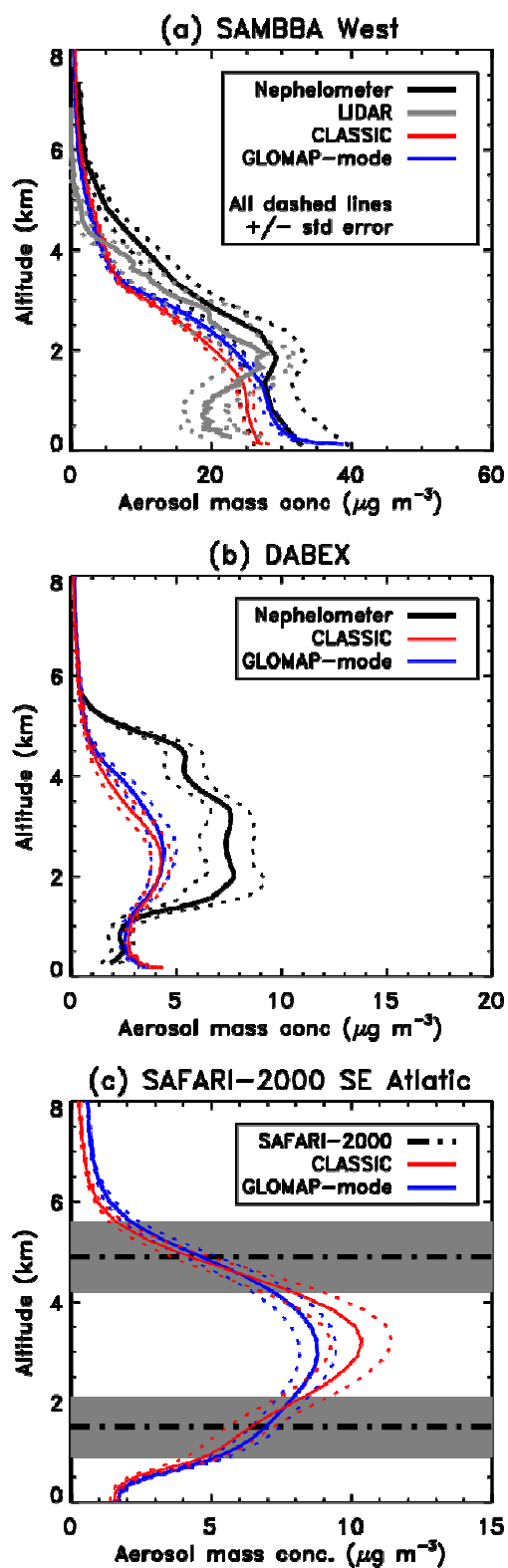
Figure 12. Seasonal cycle of moist aerosol optical properties (single scattering albedo and Ångström exponent). AERONET data from Alta Floresta (Southern Amazonia) and Mongu (Southern Africa) include all available monthly means (grey) and the long-term monthly mean (black) for months with good data coverage (see text). Co-located model data from GLOMAP-mode (red) and CLASSIC (blue) are shown taking the column average long-term monthly means.



1

2 **Figure 13.** Hygroscopic growth curves showing the increase in aerosol scattering at 550nm
3 with ambient relative humidity from a variety of observational sources and from the models.
4 The curve for CLASSIC assumes a mixture of 10 % fresh and 90 % aged BBA. The curve for
5 GLOMAP-mode is calculated based on the average composition from the four BB regions in
6 Fig. 7. The solid filled areas show the range of growth factors estimated from each
7 observation source (see text).

8





1 **Figure 14.** Vertical profiles of fine-mode aerosol mass concentration for the SAMBBA,
2 DABEX and SAFARI-2000 airborne campaigns, including model averages for CLASSIC
3 (red) and GLOMAP-mode (blue). Dashed lines show the mean +/- the standard error. Profiles
4 of mass concentrations have been estimated from campaign-averaged nephelometer (black)
5 and lidar (green) observations using the fine-mode specific scattering ($k_{\text{sca, fm}}$) and extinction
6 coefficients ($k_{\text{ext, fm}}$), respectively, derived from the in-situ aircraft observations (see the
7 second half of Table 2; $k_{\text{sca, fm}} = k_{\text{ext, fm}} * \text{SSA}$). The SAFARI-2000 observations indicate the
8 average altitude of BBA layer base and top (black dot-dashed line) +/- the standard deviation
9 (grey shading).